Otology & Neurotology
27:362–366 © 2006, Otology and Neurotology, Inc.

Three-Dimensional Analysis of Benign Paroxysmal Positional Nystagmus in a Patient with Anterior Semicircular Canal Variant

*†Takao Imai, ‡Noriaki Takeda, *Mahito Ito, §Koji Nakamae, §Hideki Sakae, ¶Hiromu Fujioka, and †Takeshi Kubo

**Department of Otolaryngology, Kansai-Rosai Hospital, Hyogo, Japan, †Department of Otolaryngology and Sensory Organ Surgery, Osaka University Graduate School of Medicine, Osaka, Japan, ‡Department of Otolaryngology, University of Tokushima School of Medicine, Tokushima, Japan, §Department of Information Systems Engineering, Osaka University Graduate School of Engineering, Osaka, Japan and ¶Department of Management and Information Sciences, Fukui University of Technology, Fukui, Japan*

Objective: To show the positional nystagmus in a patient who had suffered from benign paroxysmal positional vertigo (BPPV) that was thought to be caused by involvement of the anterior semicircular canal (ASCC) (A-BPPV).
Study Design: Retrospective case report.
Setting: City hospital.
Patient: The present study reports a rare case of A-BPPV in a 41-year-old woman.
Case Report: The patient is 41-year-old woman who developed a positional vertigo after playing volleyball on March 22, 2005 and consulted our hospital the next day. When left Dix-Hallpike maneuver was performed, she showed a positional nystagmus of which fast phase direction of the torsional component was clockwise while that of the vertical component was downward. We plotted the slow phase eye velocity of the positional nystagmus during the left Dix-Hallpike maneuver on three-dimensional coordinates that showed the axis of the positional nystagmus to be perpendicular to the plane of the right ASCC.
Conclusion: These results suggested that the patient was suffering from A-BPPV. **Key Words:** Positional nystagmus—Anterior semicircular canal—Three-dimensional coordinate—Rotation vector—Canalolithiasis.
Otol Neurotol 27:362–366, 2006.

Benign paroxysmal positional vertigo (BPPV) is the most common peripheral vestibular disease which is usually caused by involvement of the posterior semicircular canal (PSCC) (P-BPPV) (1–6). Recently, the horizontal canal type of BPPV (H-BPPV) has been recognized (7–10) and it has been reported that 5–10% of BPPV patients suffered from this type of vestibular disorder (7), but more recent studies have shown that H-BPPV is actually not rare because up to 30% of BPPV patients have been found to suffer from H-BPPV (4,6). Moreover, anterior semicircular canal (ASCC) type of BPPV (A-BPPV) has been reported (2–5,11) and because of its anatomical position, it is very difficult that canalolithiasis (1) naturally gets into ASCC. This explains why the incidence of A-BPPV is very low and why most cases of A-BPPV are transformed from P-BPPV after the canalith repositioning maneuver (12) (11). We report herein the case of a patient who has naturally suffered from A-BPPV.

Address reprint requests and correspondence to Takao Imai, M.D., Ph.D., Department of Otolaryngology, Kansai-Rosai Hospital, 3-1-69 Inabasou, Amagasaki, Hyogo 660-8511, Japan; E-mail: imaitakao@hotmail.com

PATIENT AND METHODS

We reported the case of a patient with a positional nystagmus of which fast phase direction of the torsional component was clockwise while that of the vertical component was downward when her head was brought from the sitting position down to left head hanging position (left Dix-Hallpike maneuver) (1).

All her positional nystagmus was recorded on videotape with an infrared CCD camera (*RealEyes*, Micromedical Technologies). Her left eye movements were recorded. In this paper, the description of the tridimensional eye movements was done using rotation vectors, which represent the 3-D eye positions by a single rotation. The rotation vector was given by

the axis of rotation, and its length was proportional to the size of the rotation (13). An eye position can be reached by rotating the eye from a reference position on a single axis. This eye position was represented by a vector along a single axis of which length was proportional to the angle of the rotation. The reference position was defined as the position that the eye assumes when the subject was looking straight ahead with the head kept upright while straight ahead was defined as looking at a target which was located horizontally in front of the eye (13). Using rotation vectors, Listing's law can be formulated very simply. While looking at a small target, all rotation vectors characterizing 3-D eye position lie closely scattered along a plane (13). The analysis method of the eye rotation vectors and the accuracy of this method have already been described (14,15). We converted these videotape images into 30 Hz digital ones (640*480dot) (*PCV-R63K*, SONY) and from the images, we reconstructed the space coordinates of the center of pupil and an iris freckle. These coordinates (X, Y and Z) were defined so that X-axis was parallel to the naso-occipital axis (positive forward), Y-axis parallel to the inter-aural axis (positive left), and Z-axis normal to the X-Y plane (positive upwards). X, Y and Z components mainly reflect the roll, pitch and yaw components, respectively. The rotation vector **r** describing a rotation of θ about the axis **n** is given by the formula $\mathbf{r} = \tan(\theta/2) * \mathbf{n}$, where **n** is an unit vector of which direction represents that of the axis. Because Euler angle is familiar, we used this parameter given as $2*tan^{-1}$ (magnitude of rotation vector) to represent the eye position as axis-angle representations (16,17) (Fig. 1). The rotation vector of the eye position was *r*, and using the following formula, $\omega = 2*(d\mathbf{r}/dt + \mathbf{r}\times d\mathbf{r}/dt)/(1+\mathbf{r}^2)$, we calculated the eye velocity ω around X, Y and Z axes (13). We extracted the slow phase data from nystagmic eye movement data by using the method (patent applied for) based on a fuzzy set approach (18–21).

RESULTS

Fig. 2 shows the patient's positional nystagmus during left Dix-Hallpike maneuver. Briefly, the fast phase direction of the X component, the torsional component of her positional nystagmus was clockwise, while that of the Y component, the vertical component was downward. It was reported that patients with P-BPPV showed a positional nystagmus of which fast phase direction of

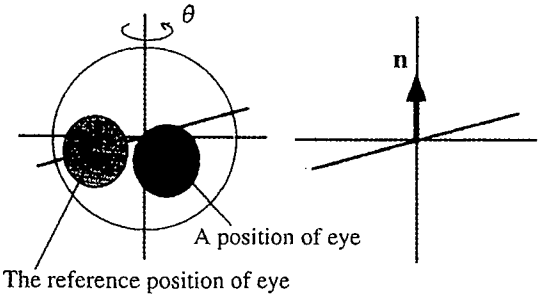

FIG. 1. Rotation vector representations. An eye position can be reached by single rotation around an axis parallel to **n** from the reference eye position. The eye position can be represented by **n** and the rotation angle θ.

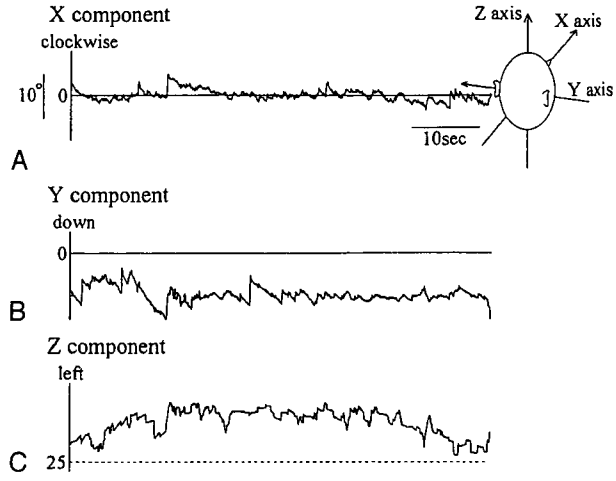

FIG. 2. Positional nystagmus during left Dix-Hallpike maneuver. (*A*), (*B*) and (*C*) represent the X, Y and Z components of the eye position, respectively. Briefly, the direction of the X component of the positional nystagmus, the torsional component was clockwise while that of the Y component, the vertical component was downward.

the X component was counterclockwise while that of the Y component was upward during left Dix-Hallpike maneuver (22). This observation is in opposition to ours. Fig. 3 shows that her positional nystagmus during right Dix-Hallpike maneuver was not clear. Fig. 4 shows the slow phase eye velocity of the rotation vector of her positional nystagmus during left Dix-Hallpike maneuver. The direction of X component of the slow phase velocity of her positional nystagmus was counterclockwise while that of the Y component was upward. In Fig. 5, slow phase eye velocities of the rotation vector of her positional nystagmus in Fig. 4 were plotted on XY, XZ and YZ planes. It was demonstrated that the axis of her

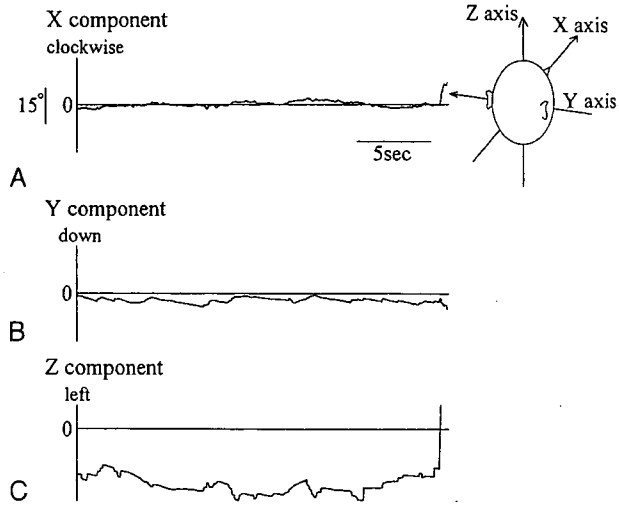

FIG. 3. Positional nystagmus during right Dix-Hallpike maneuver. (*A*), (*B*) and (*C*) represent the X, Y and Z components of the eye position, respectively. There was no clear nystagmus.

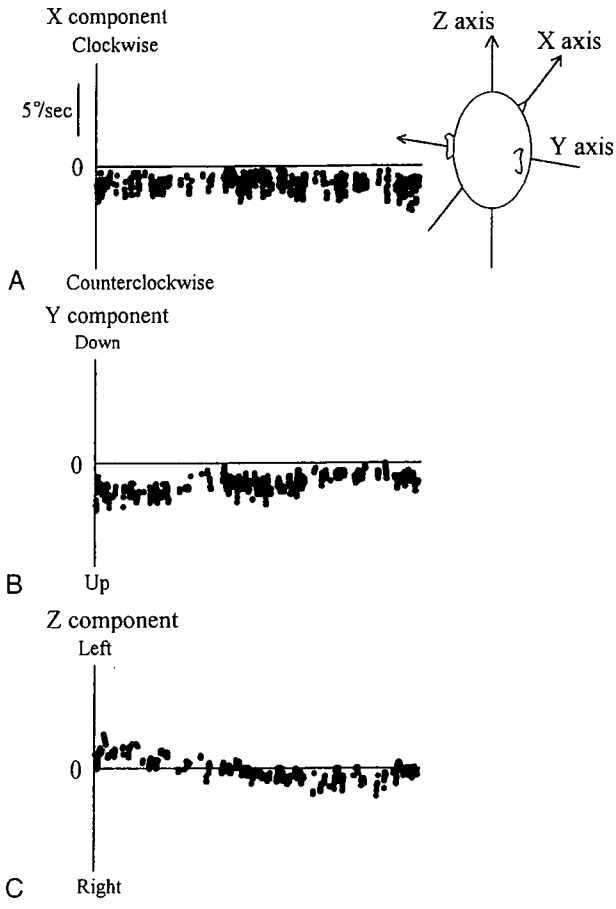

FIG. 4. Shows the slow phase eye velocity of positional nystagmus during left Dix-Hallpike maneuver. (*A*), (*B*) and (*C*) represent the X, Y and Z components of the eye position, respectively. The direction of the X component of slow phase eye velocity of positional nystagmus was counterclockwise, while that of the Y component was upward.

positional nystagmus was perpendicular to the plane of the right ASCC (23).

CASE REPORT

On March 23, 2005, a 41-year-old woman visited our hospital complaining of vertigo from the evening of March 22 when she developed vertigo after she enjoyed a volleyball game during which she rolled on the court several times to receive the ball. Her vertigo was stronger when her head was put down than raised. She was admitted to our hospital the same day and her positional vertigo gradually disappeared without canalith repositioning maneuver (12). She showed no hearing loss in any of her ears and had no other oto-neurological dysfunction, nor a canal paresis to the right or left ear irrigation with water at 20°C. The percent of canal paresis (CP%) was 4.9%. On April 19, no positional nystagmus was elicited by left Dix-Hallpike maneuver after gradually disappearing.

DISCUSSION

In this case, no canal paresis to the right or left ear was observed after irrigation with water at 20°C (24,25). This means that the functions of her lateral semicircular canals and superior vestibular nerve were normal, because the result of caloric test mainly reflects the function of lateral semicircular canals (26,27). She showed positional nystagmus of which rotational axis was perpendicular to the plane of right ASCC during left Dix-Hallpike maneuver. Aw et al showed that semicircular canal excitation is largely responsible for the alignment of the eye rotation axis (28). In this case, by left Dix-Hallpike maneuver, canalolithiasis movement excited right ASCC. This excitation is thought to be responsible for the alignment of the eye rotation axis to the axis perpendicular to the right ASCC. More, she showed no other oto-neurological dysfunction. Take a together, these results suggested that she had suffered from BPPV of which lesion was located in the right ASCC.

Herdman and Tusa reported two cases of anterior canal BPPV (11). The positioning nystagmus of one case had torsional component and the positioning nystagmus of the other case didn't have torsional component. The torsional component of the nystagmus is reported to be variable in amplitude, and often primarily downbeat. This may introduce some variability in the actual vectors of the slow phases in ASCC stimulation, as apposed to the theoretical clustering around the expected axis of the ASCC. The positioning nystagmus of our case was also primarily down beat (Fig. 2), and our rotation vectors of slow phase eye velocity clustered around the expected axis of the ASCC (Fig. 5).

BPPV is usually caused by involvement of the PSCC (1–6). Recently, A-BPPV has been recognized as a variant of positional vertigo, but its incidence is very low (2–5,11). The reason is that canalolithiasis is easier to get into PSCC than ASCC. In fact, considering the anatomy of the vestibule, PSCC is in a lower position as compared to ASCC (3,5). It is, therefore, very difficult that canalolithiasis naturally gets into ASCC. A-BPPV occurs inadvertently as a transition from typical P-BPPV to A-BPPV after canalith repositioning maneuver (11). In this case, the patient developed vertigo after playing volleyball and rolling several times on the court to receive the ball, suggesting that canalolithiasis got into ASCC following the vigorous head movements while diving to receive the ball.

She was tested by Dix-Hallpike maneuver everyday during her hospitalization, and also on March 31, April 6, and April 19. On the days other than April 19, she showed positional nystagmus of which rotational axis was perpendicular to the plane of right ASCC during left Dix-Hallpike maneuver. However, she showed no clear positional nystagmus at April 19. This means that her canalolithiasis persisted in the right ASCC from where it was directly discharged into the utricule. She had suffered from A-BPPV for 28 days, the duration of which was shorter than that of the P-BPPV that was reported to

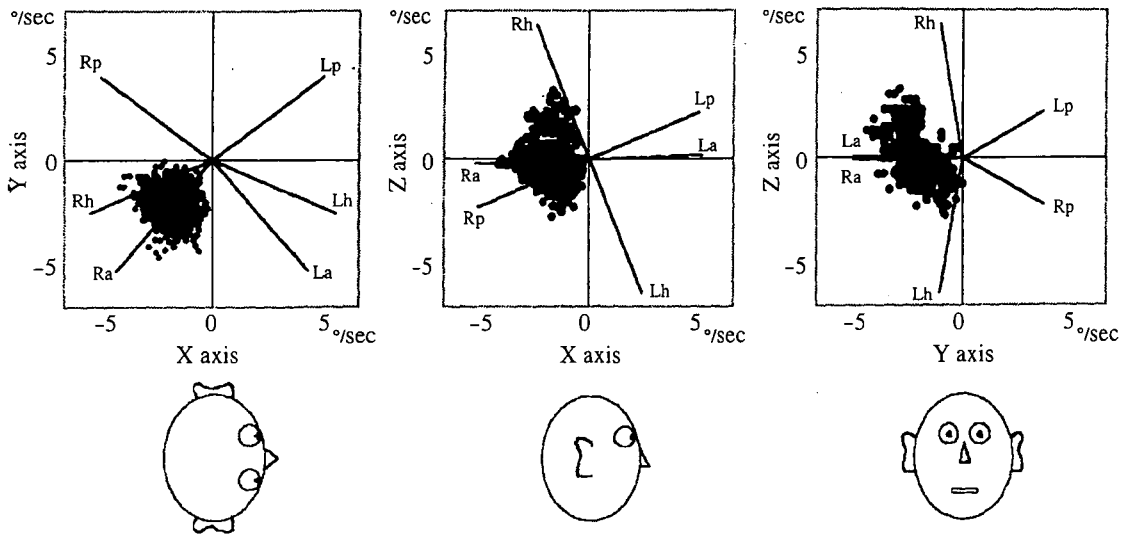

FIG. 5. Represents XY, XZ, and YZ planes on which the slow phase eye velocity data from Fig. 3 are plotted and show the different axes that are perpendicular to the following planes:
Ra: axis of the right anterior semicircular canal
Rh: axis of the right horizontal semicircular canal
Rp: axis of the right posterior semicircular canal
La: axis of the left anterior semicircular canal
Lh: axis of the left horizontal semicircular canal
Lp: axis of the left posterior semicircular canal (23).

average 39 days (6). In conclusion, our study has shown that although A-BPPV is rare, it really exists and that due to its anatomical position on the cochlea, it is easier for a canalolithiasis in the ASCC to be directly displaced into the utricule as compared to one in the PSCC.

Acknowledgments: The authors would like to thank Toru Seo, M.D., Ph. D., from Takarazuka municipal hospital for his helpful advice.

REFERENCES

1. Dix MR, Hallpike CS. Pathology, symptomatology and diagnosis of certain disorders of the vestibular system. *Proc Roy Soc Med* 1952; 45:341–54.
2. Baloh RW. Benign positional vertigo. In: Baloh RW, Halmagyi CM, eds. *Disorders of the vestibular system.* NewYork: Oxford university press; 1996:328–39.
3. Brandt T. Benign paroxysmal positioning vertigo. In: Brandt T, eds. *Vertigo: its multisensory syndromes.* 2nd ed. London: Springer-Verlag press; 1999:251–83.
4. Uno A, Uno A, Moriwaki K, et al. Clinical features of benign paroxysmalpositional vertigo. *Nippon Jibiinkoka Gakkai Kaiho* 2001; 104:9–16.
5. Parnes LS, Agrawal SK, Atlas J. Diagnosis and management of benign paroxysmal positional vertigo (BPPV). *CMAJ* 2003;169: 681–93.
6. Imai T, Ito M, Takeda N, et al. Natural course of the remission of vertigo in patients with benign paroxysmal positional vertigo. *Neurology* 2005;64:920–1.
7. McClure JA. Horizontal canal BPV. *J Otolaryngol* 1985;14: 30–5.
8. Pagnini P, Nuti D, Vannuchi P. Benign paroxysmal vertigo in the horizontal canal. *ORLJ Otorhinolaryngol Relat Spec* 1989;51: 161–70.
9. Baloh RW, Jacobson K, Horubia V. Horizontal semicircular canal variant of benign positional vertigo. *Neurology* 1993;43:2542–9.
10. Augusto PC, Giovanni V, Bruno F, et al. The treatment of horizontal canal positional vertigo: our experience in 66 cases. *Laryngoscope* 2002;112:172–8.
11. Herdman SJ, Tusa RJ. Complications of the canalith repositioning procedure. *Arch Otolaryngol Head Neck Surg* 1996;122:281–6.
12. Eply JM. The canalith repositioning procedure: for treatment of benign paroxysmal positional vertigo. *Otolaryngol Head Neck Surg* 1992;107:399–404.
13. Haslwanter T. Mathematics of three-dimensional eye rotations. *Vision Res* 1995;12:1727–39.
14. Imai T, Takada N, Morita M, et al. Rotation Vector Analysis of Eye Movement in Three Dimensions with an Infrared CCD Camera. *Acta Otolaryngol (Stockh)* 1999;119:24–8.
15. Imai T, Sekine K, Hattori K, et al. Comparing the accuracy of video-oculographyand the scleral search coil system in human eye movement analysis. *Aurisn Nasus Larynx* 2005;32:3–9.
16. Schnabolk C, Raphan T. Modeling three dimensional velocity-to-position transformation in oculomotor control. *J Neurophysiol* 1994;71:623–38.
17. Raphan T. Modeling control of eye orientation in three dimensions. I. Role of muscle pulleys in determining saccadic trajectory. *J Neurophysiol* 1998;79:2653–67.
18. Naoi K, Nakamae K, Fujioka H, et al. Three-dimensional eye movement simulator extracting instantaneous eye movement rotation axes,the plane formed by rotation axes, and innervations for eye muscles. *IEICE TRANSINF& SYST* 2003;11:2452–62.
19. Sekine K, Imai T, Nakamae K, Miura K, Fujioka H, Takeda N. Dynamics of the vestibulo-ocular reflex inpatients with the horizontal semicircular canal variant of benign paroxysmal positional vertigo. *Acta Otolaryngol* 2004;124:587–94.
20. Sekine K, Imai T, Morita M, et al. Vertical canal function in normal subjects and patients with benign paroxysmal positional-vertigo. *Acta Otolaryngol* 2004;124:1046–52.
21. Arzi Anzi M, Mignin M. A fuzzy set theoretical approach to automatic analysis of nystagmic eye movements. *IEEE Trans On Biomedical Engineering* 1987;36:954–63.

22. Imai T, Takeda N, Uno A, et al. Three-dimensional eye rotation axis analysis of benign paroxysmal positioning nystagmus. *ORL* 2002;64:417–23.
23. Blanks RHI, Curthous IS, Markham CH. Planar relationships of the semicircular canals in man. *Acta Otolaryngol (Stockh)* 1975; 80:185–96.
24. Leigh J, Zee D. The vestibular-optokinetic system. In: Leigh J, Zee D, eds. The neurology of eye movements. 3rd ed. NewYork: Oxford University press, 1999:19–150.
25. Fife TD, Tusa RJ, Furman JM, et al. Assessment: vestibular testing techniques in adults and children. *Neurology* 2000;55:1431–41.
26. Bárány R. Untersuchungen über den vom vestibulärapparatdes ohres reflektorisch ausgelösten rhythmischen nystagmus und seinebegleiterscheinungen. *Monatsschr Ohrenheilk Laryngorhinol* 1906;40:193–212.
27. Aw ST, Haslwanter T, Fetter M, Heimberger J, Todd MJ. Contribution of the vertical semicircular canals to the caloric nystagmus. *Acta Otolaryngol (Stockh)* 1998;118:618–27.
28. Aw ST, Halmagyi GM, Haslwanter T, Curthoys IS, Yavor RA, Todd MJ. Three-dimensional vector analysis of the human vestigular reflex in response to high-acceleration head rotations II. Responses in subjects with unilateral vestibular loss and selective semicircular canal occlusion. *J Neurophysiol* 1996;76: 4021–30.

ELSEVIER

Auris Nasus Larynx 34 (2007) 303–306

AURIS NASUS LARYNX
INTERNATIONAL JOURNAL OF ORL & HNS

www.elsevier.com/locate/anl

Autonomic responses during motion sickness induced by virtual reality

Seizo Ohyama [a], Suetaka Nishiike [b,*], Hiroshi Watanabe [c], Katsunori Matsuoka [c], Hironori Akizuki [a], Noriaki Takeda [a], Tamotsu Harada [b]

[a] *Department of Otolaryngology, University of Tokushima School of Medicine, Tokushima 770-0042, Japan*
[b] *Department of Otolaryngology, Kawasaki Medical School, 577 Matsushima, Kurashiki, Okayama 701-0192, Japan*
[c] *Institute for Human Science and Biomedical Engineering, National Institute of Advanced Industrial Science and Technology, Osaka 563-8577, Japan*

Received 26 May 2006; accepted 26 January 2007
Available online 1 March 2007

Abstract

Objective: To examine the development of subjective symptoms and heart rate variability (HRV) during motion sickness induced by virtual reality (VR).
Methods: Subjects were 10 healthy young volunteers. During VR immersion, subjects were immersed in a visual–vestibular conflict produced by VR. The levels of the subjective symptoms were assessed by Graybiel's and Hamilton's criteria. HRV was determined by measuring microvascular blood flow or electrocardiogram.
Results: Subjective symptoms evaluated by Graybiel's and Hamilton's criteria were gradually worsened during VR. Power spectrum analysis of HRV demonstrated a gradual increase in the low frequency but no change in the high frequency during VR. In this study, individual subjective symptoms were not correlated with the individual result of power spectrum analysis.
Conclusion: These findings indicate that there was an increase in sympathetic nervous activity, but no change in parasympathetic nervous activity during motion sickness induced by VR. Given the large inter-individual variability and the reliability of subjective measures, it is not surprising that there is scarcely a relation between the subjective symptoms and the results of power spectrum analysis.

Keywords: Autonomic function; Heart rate variability; Motion sickness; Virtual reality

1. Introduction

There are morphological and physiological connections between the vestibular and autonomic nervous system, including its sympathetic and parasympathetic divisions [1,2]. Motion sickness, which is produced by conflicting inputs from visual, vestibular and somatosensory afferents, generally carries vestibulo-autonomic responses in humans. Sympathetic (SNA) and parasympathetic nervous activity (PNA) makes frequency-specific contributions to the heart rate power spectrum [3]. Although there are several studies evaluating heart rate variability (HRV) and its power spectrum analysis in motion sickness to evaluate SNA and PNA during vestibulo-autonomic responses, these interactions are complex and have not yet been fully defined [4–6].

The VR system facilitates the coordination of incoherent visual–vestibular conflict to induce motion sickness [7]. Subjects act freely in this system, so that the experimental examination on subjects can be performed under their natural condition. In the present study, we examined alterations in HRV before, during and after visual–vestibular conflict by means of virtual reality (VR), and performed power spectrum analysis to determine changes in SNA and PNA during motion sickness.

2. Materials and methods

2.1. Subjects

Subjects were 10 healthy young volunteers (9 males and 1 female, mean age: 29.7 years old). All subjects had a normal otoneurologic examination. Informed consent was obtained

* Corresponding author. Tel.: +81 86 462 1111; fax: +81 86 464 1197.
E-mail address: nishiike@med.kawasaki-m.ac.jp (S. Nishiike).

0385-8146/$ – see front matter © 2007 Elsevier Ireland Ltd. All rights reserved.
doi:10.1016/j.anl.2007.01.002

from all subjects in the study, and all experimental procedures were approved by the Ethics Committee for Human and Animal Research of the Human Stress Signal Research Center at the National Institute of Advanced Science and Technology.

2.2. Stimulus conditions and experimental design

The VR system used in the present study was previously described [7]. It was a projection-based system that surrounds the subject with four screens: three rear projection screens for walls and a down-projection screen for a floor space 9 m^2 each (CAVE; Electronic Visualization Laboratory, University of Illinois, Chicago, IL). Subjects wore polarized glasses to resolve the stereoscopic imaginary. An electromagnetic tracking system attached to the glasses determined the location and angle of the user's head orientation.

During VR immersion for a 14-min period, subjects were immersed in a visual–vestibular conflict produced by VR [7]. The background under this condition was made by a randomized texture pattern. When subjects turned their head during this period, the background of the VR turned to a degree double that of the head movement on a vertical axis. In the previous study, this condition evoked motion sickness in humans [7]. During the VR off condition for a 7-min period before and after the VR immersion, there was no background projected on the screen.

Subjects were at work on the track of a virtual ball before VR (PRE), at the first period of VR (1ST), at the second period of VR (2ND) and after VR (POST) for each 7-min period, respectively (Fig. 1). This virtual ball task guaranteed an equal quantity of subject locomotion during both conditions. The virtual ball was regulated to rotate at a velocity of approximately 43.9°/s with a trajectory drawing a randomly distorted clockwise circle about one meter in diameter at the subject's eye level. We measured the subjects' symptoms and heart rate variability during the PRE, 1ST, 2ND and POST periods (Fig. 1).

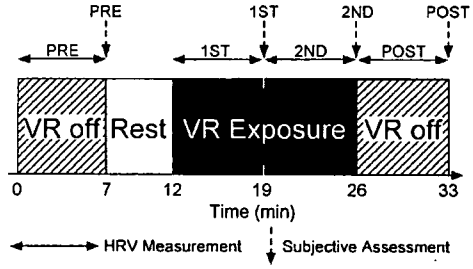

Fig. 1. Schema of time schedule. Broken line arrows indicate subjective assessments and solid line arrows indicate HRV measurement; before VR immersion (PRE), during the first period of VR immersion (1ST), at the second period of VR immersion (2ND) and after VR exit (POST).

2.3. Measures

The levels of the severity of motion sickness were given numerical scores according to Graybiel's criteria as described previously [7,8]. Total score ranges from 0 to 50. The subjective balance symptom questionnaire of Hamilton et al., was also applied [7,9,10]. Total score ranges from 0 to 16. Higher scores on both questionnaires reflected more severe symptoms.

HRV was determined by measuring microvascular blood flow in five subjects and electrocardiogram in five subjects. Microvascular blood flow was measured on the right-hand index finger nailfold skin using laser-Doppler flowmeter (Priflux PF4, Stockholm, Sweden) connected to a Finapres device (The Ohmeda 3000 Finapres Blood Pressure Monitor, Stockholm, Sweden) [11,12]. The data were forwarded to a Power Lab 4sp (AD Instruments, Castle Hill, Australia). Telemetry recordings of electrocardiogram were performed using MT11 Telemetry System (NEC Medical Systems, Tokyo). Subjects carried a small sensor (MT32&34) having three chest electrode leads for electrocardiographic recording, which was clipped to a waist belt. The data were transmitted to a receiver (MR34), forwarding them to a Power Lab 4sp.

The signal was then digitalized by the Power Lab 4sp. The cardiac tachogram was calculated using a Chart Version 4.02 (AD Instruments, Castle Hill, Australia) on a Macintosh computer. HRV was analyzed using HRV extension version 4.0 (AD Instruments, Castle Hill, Australia) at a sampling frequency of 1 kHz for each 7-min recording [11,13]. Power spectrum analysis in the frequency domain was performed by fast Fourier transformation. The low frequency power component (LP) of the HRV power spectrum (0.04–0.15 Hz) is generally accepted as a measure of both SNA and PNA and high frequency power component (HP) (0.15–0.40 Hz) as a pure measure of PNA [11,14,15]. The ratio of LP or HP to the total power spectrum (TP) is also used as an indicator of SNA/PNA or SNA to correct for baseline differences in HR between groups [11].

2.4. Statistical analysis

Analysis of variance (one factor of ANOVA with repeated measures) was used for analyzing the subjective scores and power spectrum analysis in subjects. The data of four groups (PRE, 1ST, 2ND and POST) were compared with post hoc Scheffé's test. The correlation between subjective measures and LP/TP was analyzed by Pearson correlation test.

3. Results

Under the visual–vestibular conflict produced by VR, the score of Graybiel's criteria gradually increased and showed a significantly higher score during the 2ND period of VR

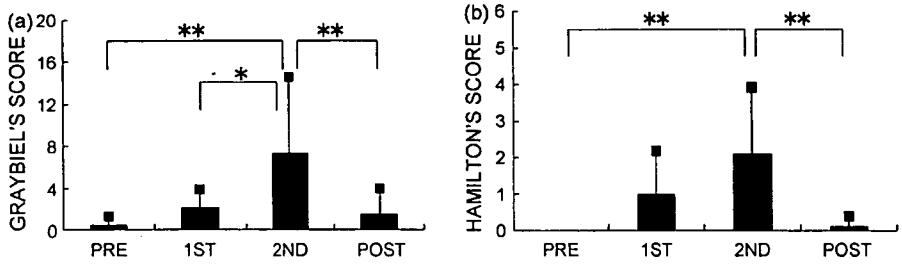

Fig. 2. The severity of the Graybiel's criteria (a) and Hamilton's criteria (b) on immersion in VR. $^{*}p < 0.05$. $^{**}p < 0.01$. Error bar: S.D.

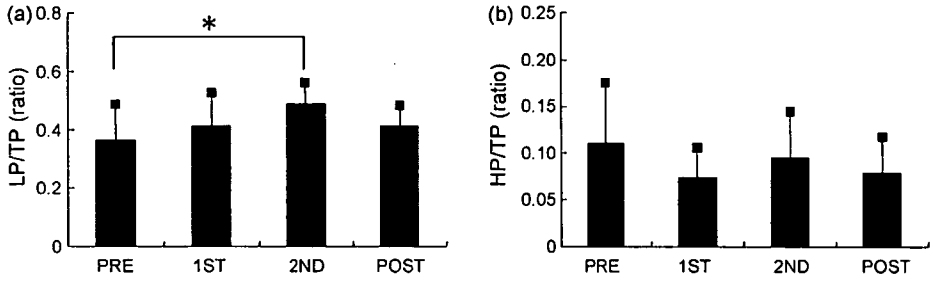

Fig. 3. The ratio of LP/TP (a) and HP/TP (b) on immersion in VR. $^{*}p < 0.05$. Error bar: S.D.

(Fig. 2). During the POST period, the score for motion sickness was decreased. The score for Hamilton's criteria under the visual–vestibular conflict showed the same changes over time as Graybiel's score (Fig. 2).

Similarly the LP/TP was gradually increased and showed a significantly higher score at the 2ND period of VR. During the POST period, the LP/TP was decreased (Fig. 3). The HP/TP was not significantly changed during or after VR (Fig. 3).

Large inter-individual variability was observed in measures for subjective symptoms. The ranges of individual scores during the 2ND period of VR in Graybiel's questionnaire and Hamilton's questionnaire were 0.00–20.00 and 0.00–6.00, respectively. However, the ranges of LP/TP at the 2ND period of the VR were not so large: 0.41–0.59. The individual Graybiel's score and Hamilton's score at any period were not correlated with LP/TP (the correlation index = 0.21 and 0.29, $p = 0.18$ and 0.06, respectively).

4. Discussion

In the present study, power spectrum analysis of HRV was performed on the microvascular blood flow or electrocardiogram recorded before, 1ST, 2ND period, and after visual–vestibular conflict produced by VR. Subjective symptoms evaluated by Graybiel's and Hamilton's criteria were gradually worsened during the VR, indicating that this condition induced motion sickness in subjects. We observed an increase in the power spectrum density of HRV in the low frequency and no significant change in the high frequency, suggesting increased sympathetic activity during motion sickness.

In the previous study, we examined the development of subjective and objective symptoms using virtual reality [7]. Subjects were immersed in two different VR conditions. One was a visual–vestibular conflict (mismatch) condition; when subjects turned their heads, the background of the VR turned to a degree double that of the head movement on a vertical axis. The other was the Control condition; an interactive computer graphics synchronizing the background image proportionally to the subject motion. The subjective symptoms evaluated by Graybiel's and Hamilton's criteria gradually worsened under the mismatch condition. Under the Control condition, these were not significantly changed. Thus, we concluded in the previous study that the mismatch condition induced by VR provoked motion sickness in humans.

The power spectrum density of the HRV at the low frequency is influenced both by the SNA and PNA [3,16]. That at the high frequency is a pure measure of PNA [11,14,15]. In this study, there was no significant change in the power spectrum density of the HRV at the high frequency, indicating that there was no remarkable change in parasympathetic tone during motion sickness. This finding suggests that the increase in the low frequency peak is due to an increase in SNA. The present findings were supported by previous reports examining HRV during motion sickness: a decrease in PNA during motion sickness reported by some authors evaluating alterations in HRV [5,6] and an increase in heart rate in previous reports [17] may be explained by sympathetic arousal and/or parasympathetic attenuation.

Ishii et al. also examined HRV in monkeys during motion sickness, but reported an increase in PNA during the development of motion sickness. Doweck et al. [5] and Hu

et al. [6] explained this inconsistency by differences in the study design. The study by Ishii et al. [4] employed monkeys, whereas in our and other studies humans were the subjects [17]. A second difference is the end point of the study [5]; Ishii's group [4] based their criterion for motion sickness on vomiting, Doweck's group [5] on imminent emesis; whereas in our study, all subjects accomplished tasks during motion sickness and subjective sensational emesis may have been weaker than those in other studies.

Koch et al. [18] reported that increased plasma levels of epinephrine and norepinephrine in subjects with experimental vection-induced motion sickness. Gordon et al. [19] reported a decrease in salivary flow rate and an increase in potassium concentration explained by sympathetic activation. These findings also support the results of HRV measurement. Parker and Wilsoncroft [20] indicated that increased sympathetic tone tended to reduce autonomic reactions to motion stimuli. This seems to be supported by the findings of Himi et al. [21]: the activity of the sympathetic nervous system in the nausea group was relatively lower before stimulus and significantly higher during motion stimuli; that in the non-nausea group was relatively higher before the stimuli and did not show any change during stimulation. They suggested that symptoms related to the sympathetic nervous system may actually be defensive reactions against the sensation of nausea [21].

In this study, there was no correlation of individual scores on Graybiel's or Hamilton's criteria to individual LP/TP during any periods. Given the large inter-individual variability and the reliability of subjective measures, it is not surprising that there is scarcely a relation between the two measures. Previous reports also indicated a low relation between subjective reports of motion sickness or balance-related symptoms and postural instability [22]. It has been reported that the interaction between spatial orientation perception and reflexive eye movements are also contradictory [23,24].

5. Conclusion

Power spectrum analysis of the HRV demonstrated that provocation of motion sickness in humans cause sympathetic arousal, expressed by an increase at the LP/TP and there was no change at the HP/TP. The individual subjective symptoms were not correlated with individual sympathetic tones.

References

[1] Money KE. Motion sickness. Physiol Rev 1970;50:1–39.
[2] Previc FH. Do the organs of the labyrinth differentially influence the sympathetic and parasympathetic systems? Neurosci Biobehav Rev 1993;17:397–404.
[3] Akselrod S, Gordon D, Ubel FA, Shannon DC, Berger AC, Cohen RJ. Power spectrum analysis of heart rate fluctuation: a quantitative probe of beat-to-beat cardiovascular control. Science 1981;213:220–2.
[4] Ishii M, Igarashi M, Patel S, Himi T, Kulecz W. Autonomic effects on R–R variations of the heart rate in the squirrel monkeys. Am J Otolaryngol 1987;8:144–8.
[5] Doweck I, Gordon CR, Shlitner A, Spitzer O, Gonen A, Binah O, et al. Alterations in R–R variability associated with experimental motion sickness. J Auton Nerv Syst 1997;67:31–7.
[6] Hu S, Grant WF, Stern RM, Koch KL. Motion sickness severity and physiological correlates during repeated exposures to a rotating optokinetic drum. Aviat Space Environ Med 1991;62:308–14.
[7] Akiduki H, Nishiike S, Watanabe H, Matsuoka K, Kubo T, Takeda N. Visual–vestibular conflict induced by virtual reality in humans. Neurosci Lett 2003;340:197–200.
[8] Graybiel A, Wood CD, Miller EF, Cramer DB. Diagnostic criteria for grading the severity of acute motion sickness. Aerospace Med 1968;39:453–5.
[9] Hamilton KM, Kantor L, Magee LE. Limitations of postural equilibrium tests for examining simulator sickness. Aviat Space Environ Med 1989;60:246–51.
[10] Cobb SVG, Nochols SC. Static posture tests for the assessment of postural instability after virtual environment use.. Brain Res Bull 1998;47:459–64.
[11] Berakis A, Williams TJ, Naughton MT, Martin JH, Muhlmann M, Krum H. Altered sympathetic and parasympathetic activity in lung transplantation patients at rest and following autonomic perturbation. Chest 2002;122:1192–9.
[12] Maver J, Štrucl M, Accetto R. Autonomic nervous system activity in normotensive subjects with a family history of hypertension. Clin Auton Res 2004;14:369–75.
[13] Pliquett RU, Cornish KG, Zucker IH. Statin therapy restores sympathovagal balance in experimental heart failure. J Appl Physiol 2003;95:700–4.
[14] Eckberg DL, Kifle YT, Roberts VL. Phase relationship between normal human respiration and baroreflex responsiveness. J Physiol 1980;304:489–502.
[15] Malik M, Camm AJ. Components of heart rate variability—what they really mean and what we really measure. Am J Cardiol 1993;72:821–2.
[16] Kitney RI, Rompelman O. The study of heart rate variability. Oxford: Clarendon Press; 1980.
[17] Cowings PS, Suter S, Toscano WB, Kamiya J, Naifeh K. General autonomic components of motion sickness. Psychophysiology 1986;23:542–51.
[18] Koch KL, Stern RM, Vasey MW, Seaton JF, Demers LM, Harrison TS. Neuroendocrine and gastric myoelectrical responses to illusory self-motion in humans. Am J Physiol 1990;258:E304–10.
[19] Gordon CR, Jackman Y, Ben-Aryeh H, Doweck I, Spitzer O, Szargel R, et al. Salivary secretion and seasickness susceptibility. Aviat Space Environ Med 1992;63:356–9.
[20] Parker DM, Wilsoncroft WE. Intensity of motion sickness symptoms as a function of apparent autonomic balance. J Gen Psychol 1978;98:253–7.
[21] Himi N, Koga T, Nakamura E, Kobashi M, Yamane M, Tsujioka K. Differences in autonomic responses between subjects with and without nausea while watching an irregularly oscillating video. Auton Neurosci 2004;116:46–53.
[22] Thomley K, Kennedy RS, Bittner Jr A. Development of postural equilibrium tests for examining environmental effects. Percept Mot Skills 1986;63:1160–7.
[23] Ivanenko Y, Grasso R, Berthoz A. Spatial orientation in humans: perception of angular whole-body displacements in two-dimensional trajectories. Exp Brain Res 1997;117:419–27.
[24] Ivanenko YP, Viaud-Delmon I, Siegler I, Israel I, Berthoz A. The vestibulo-ocular reflex and angular displacement perception in darkness in humans: adaptation to a virtual reality. Neurosci Lett 1998; 241:167–70.

ORL

ORL 2005;67:289–293
DOI: 10.1159/000089410

Published online: December 15, 2005

Ménière's Disease Is Associated with Single Nucleotide Polymorphisms in the Human Potassium Channel Genes, *KCNE1* and *KCNE3*

Katsumi Doi Takashi Sato Toshihiro Kuramasu Hiroshi Hibino
Tadashi Kitahara Arata Horii Naoki Matsushiro Yuka Fuse Takeshi Kubo

Department of Otolaryngology and Sensory Organ Surgery, Osaka University Graduate School of Medicine, Suita, Osaka, Japan

Key Words
Ménière's disease · Genetic association study · Mutation · Polymorphism · Single nucleotide polymorphisms · *KCNE* genes · Potassium channel

Abstract
Although the bases for both the sporadic and inherited forms of Ménière's disease (MD) remain undefined, it is likely to be multifactorial, one of the factors being a genetic predisposition. Recently, genetic association studies on complex diseases have become very popular and most of them are case-control studies using single nucleotide polymorphisms (SNPs) as markers. Mutations/polymorphisms in *KCNE* potassium channel genes might play a causative role in MD, because KCNE potassium channels have been suggested to be present and active in transmembrane ion and water transports in the inner ear. In the present study, to identify MD susceptibility genes, we have conducted a genetic association study with optimized sampling, optimized phenotyping/genotyping, and a selection of *KCNE* genes as the candidate genes. The SNPs analyses identified 112G/A SNP in the *KCNE1* gene and 198T/C SNP in the *KCNE3* gene in 63 definite MD cases as well as 205 and 237 non-MD control subjects. For both *KCNE1* and *KCNE3* genes, a significant difference in frequency of each SNP was confirmed between MD cases and non-MD control subjects. The result indicates that 112G/A SNP in the *KCNE1* gene and 198T/C SNP in the *KCNE3* gene could determine an increased susceptibility to develop MD.

Introduction

Ménière's disease (MD) is defined as an idiopathic disorder of the inner ear characterized by the triad of tinnitus, vertigo, and sensorineural hearing loss. Approximately 90% of MD cases are sporadic and the remaining 10% of MD cases are genetic. Although the bases for both the sporadic and inherited forms of MD remain undefined, it is likely to be multifactorial, one of the factors being a genetic predisposition [1]. Recently, genetic association studies on complex disease have become very popular and most of them are case-control studies using single nucleotide polymorphisms (SNPs) as markers [2]. However, there has been concern about limitations of this type of study, which can lead to poor reproducibility, false positive and false negative results. The poor reproducibility has most commonly been associated with small sample size, population stratification, and poor selection of genes or SNPs [2].

KARGER

Fax +41 61 306 12 34
E-Mail karger@karger.ch
www.karger.com

0301–1569/05/0675–0289$22.00/0

Accessible online at:
www.karger.com/orl

Katsumi Doi, MD
Department of Otolaryngology and Sensory Organ Surgery
Osaka University Graduate School of Medicine
Yamadaoka 2-2, Suita, Osaka 565-0871 (Japan)
Tel. +81 6 6879 3951, Fax +81 6 6879 3959, E-Mail kdoi@ent.med.osaka-u.ac.jp

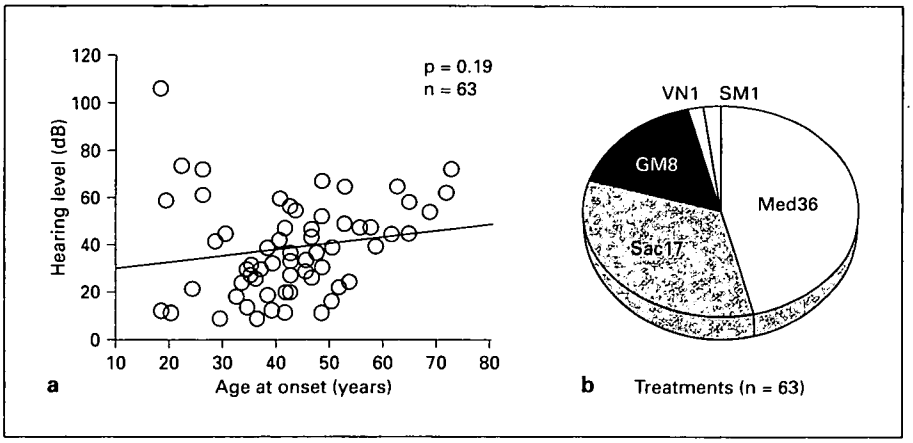

Fig. 1. Phenotypes (**a**) and treatments (**b**) of 63 cases with definite MD. Med = Medical treatments; Sac = endolymphatic sac surgery; GM = intratympanic gentamicin perfusion; VN = vestibular neurectomy; SM = semicircular canal streptomycin perfusion.

KCNE potassium channels (KCNE1–5) associated with KCNQ potassium channels are known to play an essential role in transepithelial ion and water transport in several organs including heart, kidney, colon, and small intestine [3]. In the intestine, *KCNE3* and *KCNQ1* mRNAs are colocalized in crypt cells and the assembled heteromeric KCNE3/KCNQ1 channel has a critical role in the regulation of cyclic AMP-stimulated chloride and water transport through the epithelial membrane [4]. In the inner ear, the expression of KCNE1 channel has been confirmed in the stria vascularis and null mutation of this gene causes an abnormal development of the endolymphatic system in the mouse cochlea accompanied by severe deafness [5]. Mutations in the *KCNE1* gene have been linked to some forms of cardiac arrhythmia, including Jervell and Lange-Nielsen syndrome with severe congenital deafness and long QT syndrome [6, 7].

RT-PCR amplification and direct sequencing confirmed the dominant expression of *KCNE1* mRNA in the rat cochlea and that of *KCNE3* mRNA in the endolymphatic sac [8]. IH and ISH studies could demonstrate that the KCNE1 channel was mainly expressed in the marginal cells of the stria vascularis while the KCNE3 channel was intensely expressed in the epithelium of the distal portion of the endolymphatic sac [8]. These results indicate that KCNE channels could be active in transmembrane ion and water transport in the inner ear and that mutations/polymorphisms in *KCNE* genes might play a causative role in MD. In the present study, to identify MD susceptibility genes, we have conducted a genetic association study with optimized sampling (large sample size), optimized phenotyping (definite MD), optimized genotyping (full sequencing), appropriate interpretation and a selection of *KCNE* genes as the candidate genes.

Materials and Methods

For SNP analyses, DNAs were extracted and prepared from lymphocytes of 63 'definite' MD cases (18 males and 45 females; mean age 42.5 years) according to the diagnostic scale of the AAO-HNS 1995 [9]. No correlation was detected between the averaged hearing level (0.5, 1, 2 kHz) of the 63 MD cases at their first appearances and the age at onset (fig. 1a). Thirty-six out of the 63 MD cases (57%) received medical treatments and the remaining 27 cases (43%) received several surgical treatments including endolymphatic sac surgery, aminoglycoside perfusion, and vestibular neurectomy (fig. 1b).

SNP analyses were performed by permission of RBI of Osaka University with written informed consent. DNA samples extracted from 237 normal non-MD subjects (68 males and 169 females, mean age 35.8 years) were used as controls in *KCNE1* SNP analysis and DNA samples from 205 non-MD control subjects (52 males and 153 females, mean age 36.5 years) were used in *KCNE3* SNP analysis. There was no statistical difference in the background of participants including age and sex between MD cases and non-MD control subjects (t test; $p > 0.1$). Full coding regions of both *KCNE1* and *KCNE3* genes were sequenced for each DNA sample and the entire nucleotide sequences were compared to those in the human genome/SNP database [10, 11]. Chi-square test combined with Fisher's exact test was used for the statistic analysis where a p level <0.05 was considered as significant.

Results

Genetic analyses confirmed 112G/A SNP in the *KCNE1* gene and 198T/C SNP in the *KCNE3* gene: 112G homozygosity, 112A homozygosity, and 112G/A heterozygosity were identified in the *KCNE1* gene, while 198T homozygosity, 198C homozygosity, and 198T/C heterozygosity were identified in the *KCNE3* gene (fig. 2a, b). An amino acid change (serine/glycine at position 38; S38G) in the KCNE1 channel can be caused by 112G/A

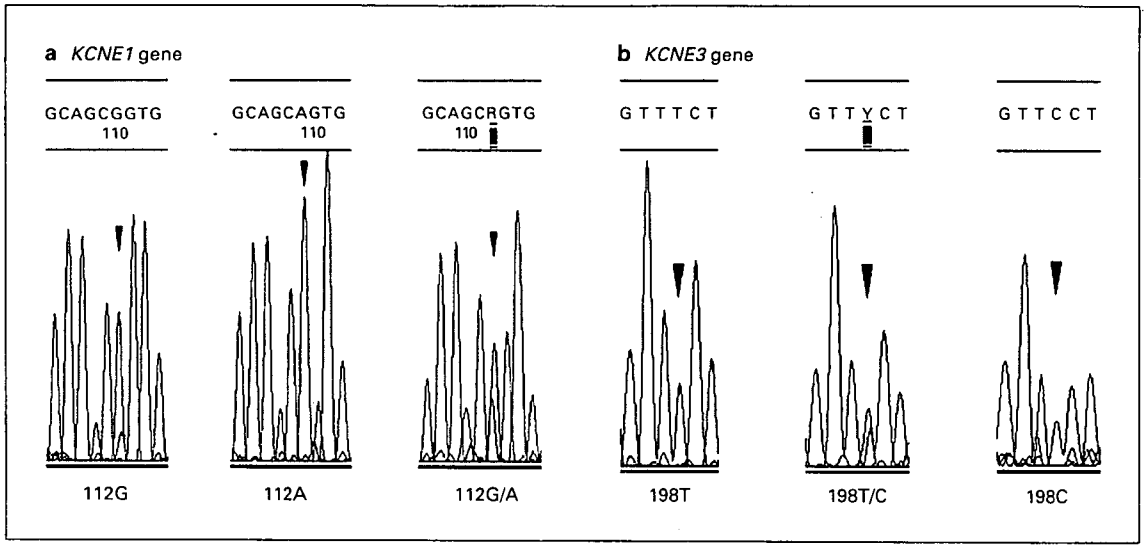

Fig. 2. Identified SNPs in *KCNE1* and *KCNE3* genes. **a** 112G homozygosity, 112A homozygosity, and 112G/A heterozygosity in the *KCNE1* gene. **b** 198T homozygosity, 198C homozygosity, and 198T/C heterozygosity in the *KCNE3* gene.

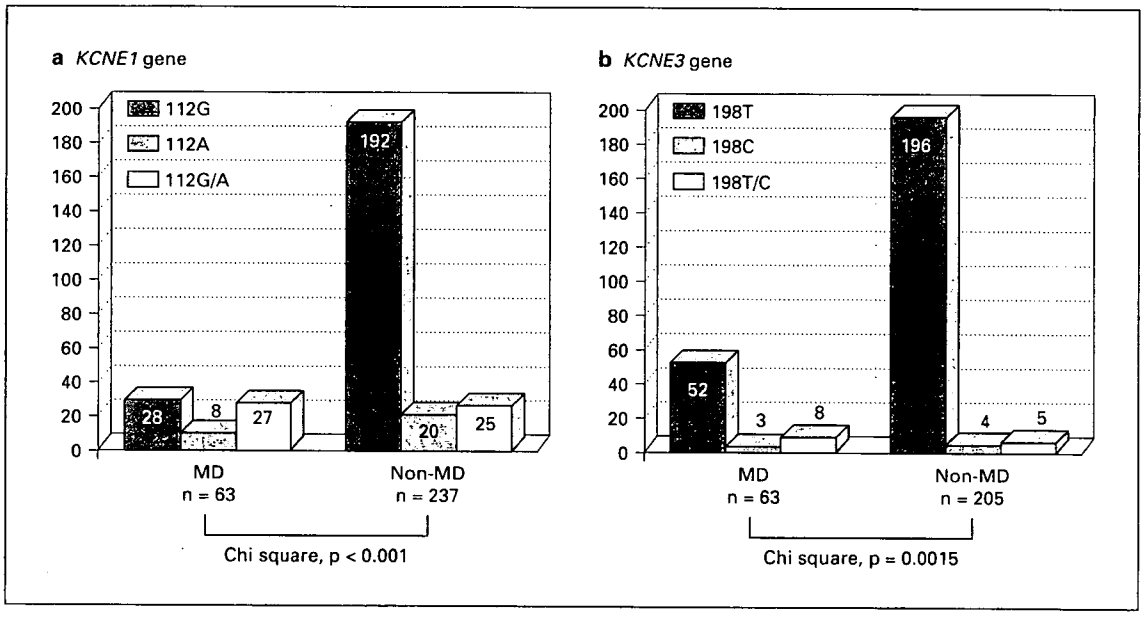

Fig. 3. Frequencies of SNPs in *KCNE1* and *KCNE3* genes. **a** 112G/A SNP in the *KCNE1* gene in 63 MD cases and 237 non-MD control subjects. **b** 198T/C SNP in the *KCNE3* gene in 63 MD cases and 205 non-MD control subjects.

SNP in the *KCNE1* gene. No amino acid change (phenylalanine at position 66; F66) in the KCNE3 channel can be produced by 198T/C SNP in the *KCNE3* gene.

As for 112G/A SNP in the *KCNE1* gene, 44.4% (28/63) of MD cases had 112G homozygosity and the remaining 55.6% (35/63) had 112A homozygosity or 112G/A heterozygosity (112A on one or both alleles; fig. 3a). In contrast, 81% (192/237) of non-MD control subjects had 112G homozygosity and the remaining 19% (45/237) had 112A homozygosity or 112G/A heterozygosity (fig.

3a). The frequency of 112G/A SNP in the *KCNE1* gene was significantly different between MD cases and non-MD control subjects ($p < 0.001$). As for 198T/C SNP in the *KCNE3* gene, 82.5% (52/63) of MD cases had 198T homozygosity and the remaining 17.5% (11/63) had 198C homozygosity or 198T/C heterozygosity (198C on one or both alleles; fig. 3b). In contrast, 95.6% (196/205) of non-MD control subjects had 198T homozygosity and the remaining 4.4% (9/205) had 198C homozygosity or 198T/C heterozygosity (fig. 3b). The frequency of 198T/C SNP in the *KCNE3* gene was also significantly different between MD cases and non-MD control subjects ($p = 0.0015$).

Discussion

The SNP analyses identified 112G/A SNP in the *KCNE1* gene and 198T/C SNP in the *KCNE3* gene in MD cases as well as non-MD control subjects. For both *KCNE1* and *KCNE3* genes, a significant difference in frequency of each SNP was confirmed between MD cases and non-MD control subjects: a high frequency of 112A homozygosity or 112G/A heterozygosity (112A on one or both alleles) in the *KCNE1* gene and a high frequency of 198C homozygosity or 198T/C heterozygosity (198C on one or both alleles) in the *KCNE3* gene could be detected in MD cases. The result indicates that 112G/A SNP in the *KCNE1* gene and 198T/C SNP in the *KCNE3* gene could determine an increased susceptibility to develop MD.

Mutations and polymorphisms in *KCNE* potassium channel genes can have significant effects on human physiology, such as fluid homeostasis, signaling in nervous tissue, and muscular contraction, and have been linked to several inherited and acquired human diseases [3]. In the inner ear, the expression of the KCNE1 channel has been confirmed in the stria vascularis and null mutation of this gene causes an abnormal development of the endolymphatic system in the mouse cochlea accompanied by deafness [5]. Mutations in the *KCNE1* gene have been linked to some forms of cardiac arrhythmia, including Jervell and Lange-Nielsen syndrome with severe congenital deafness and long QT syndrome [6, 7]. We have confirmed the dominant expression of *KCNE3* mRNA/KCNE3 channel in the epithelium of the distal portion of the endolymphatic sac [8] where passive and active volume regulation of the endolymph should occur. Considering that KCNE channels have an essential role in transepithelial ion and water transport [3] and that both KCNE1 and KCNE3 channels are intensely expressed in the epithelia of the stria vascularis and the endolymphatic sac [5, 8], it is quite likely that mutations/polymorphisms in *KCNE1* and *KCNE3* genes might lead to the cause of MD.

An amino acid change (S38G) in KCNE1 channel can be caused by 112G/A SNP in the *KCNE1* gene, while no amino acid change (F66) in KCNE3 channel can be produced by 198T/C SNP in the *KCNE3* gene. According to the alignment of amino acid sequences encoded by human *KCNE1–5* potassium channel genes, S38 within the predicted extracellular portion of *KCNE1* is conserved in *KCNE1* and *KCNE4* genes while F66 within the predicted transmembrane domain of *KCNE3* is not conserved among *KCNE1–5* genes. Future study should determine how possible alterations of the primary and secondary structures of KCNE channels caused by these two SNPs affect the physiological properties of KCNE channels in the inner ear.

The etiology of MD is likely to be multifactorial, with one of the factors being a genetic predisposition. Recent studies suggest that the *COCH* gene, HLA class I and II antigens, and antiquitin might be among the genetic factors contributing to familial and sporadic MD [12–14]. Analysis of candidate genes to reveal the genetic bases for MD has just been initiated and future studies should identify novel mutations/polymorphisms in several candidate genes for both the sporadic and inherited forms of MD, which might lead to a more precise understanding of genotype-phenotype correlations in MD. In the future, with gene-based MD diagnosis, we must be able to predict the development of MD, prevent the attack of MD, and also be able to know the responses to medical and surgical treatments in each MD case. The present study first succeeds to identify both *KCNE1* and *KCNE3* genes as the susceptibility genes for sporadic forms of MD.

Acknowledgment

This study was supported by Health and Labor Sciences Research Grants in Japan (Research on Measures for Intractable Diseases).

References

1 Morrison AW: Anticipation in Meniere's disease. J Laryngol Otol 1995;109:499–502.
2 Hegele RA: SNP judgments and freedom of association. Arterioscler Thromb Vasc Biol 2002;22:1058–1061.
3 Abbott GW, Goldstein SAN: Physiology and pathophysiology of the MinK-related peptides (MiRPs). Mol Interv 2001;1:95–107.
4 Schroeder BC, Waldegger S, Fehr S, Bleich M, Warth R, Greger R, Jentsch TJ: A constitutively open potassium channel formed by KCNE1 and KCNE3. Nature 2000;403:196–199.
5 Vetter DE, Mann JR, Wangemann P, Liu J, McLaughlin KJ, Lesage F, Marcus DC, Lazdunski M, Heinemann SF, Barhanin J: Inner ear defects induced by null mutation of the IsK gene. Neuron 1996;17:1251–1264.
6 Schulze-Bahr E, Wang Q, Wedekind H, Haverkamp W, Chen Q, Sun Y: KCNE1 mutations cause Jervell and Lange-Nielsen syndrome. Nat Genet 1997;17:267–268.
7 Abbott GW, Sesti F, Splawski I, Buck ME, Lehmann MH, Timothy KW, Keating MT, Goldstein SAN: MiRP1 forms IKr potassium channels with HERG and is associated with cardiac arrhythmia. Cell 1999;97:175–187.
8 Doi K, Sato T, Kuramasu T, Matsushiro N, Fuse Y, Kubo T: Single nucleotide polymorphism (SNP) analyses of genes encoding KCNE potassium channels in Meniere's disease; in Meniere's Disease and Inner Ear Homeostasis Disorders, in press.
9 Committee on Hearing and Equilibrium: Committee on Hearing and Equilibrium guidelines for the diagnosis and evaluation of therapy in Menière's disease. Otolaryngol Head Neck Surg 1995;113:181–185.
10 http://www.ncbi.nlm.nih.gov/projects/SNP/
11 http://snp.ims.u-tokyo.ac.jp/
12 Lemaire FX, Feenstra L, Huygen PL, Fransen E, Devriendt K, Van Camp G, Vantrappen G, Cremers CWRJ: Progressive late-onset sensorineural hearing loss and vestibular impairment with vertigo (DFNA9/COCH): longitudinal analyses in a Belgian family. Otol Neurotol 2003;24:743–748.
13 Lopez-Escamez JA, Lopez-Nevot A, Cortes R, Ramal L, Lopez-Nevot MA: Expression of A, B, C, and DR antigens in definite Meniere's disease in a Spanish population. Eur Arch Otorhinolaryngol 2002;259:347–350.
14 Lynch M, Cameron TL, Knight M, Kwok TY, Thomas P, Forrest SM, Giersch ABS, Briggs RJS, Pyman BC: Structural mutational analysis of antiquitin as a candidate gene for Meniere's disease. Am J Med Genet 2002;110:397–399.

Am J Physiol Cell Physiol 291: C1038–C1048, 2006.
First published July 5, 2006; doi:10.1152/ajpcell.00266.2006.

Gastric type H^+,K^+-ATPase in the cochlear lateral wall is critically involved in formation of the endocochlear potential

Toshiaki Shibata,[1,3] Hiroshi Hibino,[1] Katsumi Doi,[2] Toshihiro Suzuki,[3] Yasuo Hisa,[3] and Yoshihisa Kurachi[1]

[1]*Division of Molecular and Cellular Pharmacology, Department of Pharmacology, and* [2]*Department of Otolaryngology, Graduate School of Medicine, Osaka University, Suita, Osaka; and* [3]*Department of Otolaryngology, Kyoto Prefectural University of Medicine, Kyoto, Japan*

Submitted 13 May 2006; accepted in final form 25 June 2006

Shibata, Toshiaki, Hiroshi Hibino, Katsumi Doi, Toshihiro Suzuki, Yasuo Hisa, and Yoshihisa Kurachi. Gastric type H^+,K^+-ATPase in the cochlear lateral wall is critically involved in formation of the endocochlear potential. *Am J Physiol Cell Physiol* 291: C1038–C1048, 2006. First published July 5, 2006; doi:10.1152/ajpcell.00266.2006.— Cochlear endolymph has a highly positive potential of approximately +80 mV known as the endocochlear potential (EP). The EP is essential for hearing and is maintained by K^+ circulation from perilymph to endolymph through the cochlear lateral wall. Various K^+ transport apparatuses such as the Na^+,K^+-ATPase, the Na^+-K^+-$2Cl^-$ cotransporter, and the K^+ channels Kir4.1 and KCNQ1/KCNE1 are expressed in the lateral wall and are known to play indispensable roles in cochlear K^+ circulation. The gastric type of the H^+,K^+-ATPase was also shown to be expressed in the cochlear lateral wall (Lecain E, Robert JC, Thomas A, and Tran Ba Huy P. *Hear Res* 149: 147–154, 2000), but its functional role has not been well studied. In this study we examined the precise localization of H^+,K^+-ATPase in the cochlea and its involvement in formation of EP. RT-PCR analysis showed that the cochlea expressed mRNAs of gastric α_1-, but not colonic α_2-, and β-subunits of H^+,K^+-ATPase. Immunolabeling of an antibody specific to the α_1 subunit was detected in type II, IV, and V fibrocytes distributed in the spiral ligament of the lateral wall and in the spiral limbus. Strong immunoreactivity was also found in the stria vascularis. Immunoelectron microscopic examination exhibited that the H^+,K^+-ATPase was localized exclusively at the basolateral site of strial marginal cells. Application of Sch-28080, a specific inhibitor of gastric H^+,K^+-ATPase, to the spiral ligament as well as to the stria vascularis caused prominent reduction of EP. These results may imply that the H^+,K^+-ATPase in the cochlear lateral wall is crucial for K^+ circulation and thus plays a critical role in generation of EP.

hydrogen, potassium-adenosine triphosphatase; stria vascularis; spiral ligament

THE COCHLEA OF THE INTERNAL EAR is a peripheral organ that amplifies and transforms the sound-derived mechanical signal to an electrical one, which will be transmitted to the brain. This transformation is performed in the cochlear hair cells, the primary receptor for hearing. The hair cells are bathed in two distinct types of extracellular fluid: perilymph and endolymph. The ionic composition of perilymph is identical to that of ordinary extracellular solution. On the other hand, endolymph contains 150 mM K^+, 2 mM Na^+, and 20 μM Ca^{2+} and has surprisingly high potential with reference to the body fluid of approximately +80 mV, which is known as the endocochlear potential (EP) (86, 87). While the basolateral side of a hair cell is bathed in perilymph, its apical membrane, which harbors the hair bundles, is exposed to endolymph. The sound-driven vibration of the basilar membrane deflects the hair bundles and opens mechanosensitive channels at the top of their cilia, which results in influx of K^+ to the hair cells and thus their depolarization (30). By forming a large driving force for K^+ influx, EP directly contributes to the high sensitivity of the hair cells to mechanical stimulation.

It is assumed that K^+ circulation from perilymph to endolymph through the cochlear lateral wall is essential to establish the high K^+ concentration ($[K^+]$) in endolymph and EP (90). The lateral wall is divided into two components, *1*) the spiral ligament, a connective tissue comprising several types of fibrocytes, and *2*) the stria vascularis, an epithelial tissue containing marginal, intermediate, and basal cells. K^+ secreted from the hair cells is transported to the endolymphatic space via the epithelium on the basilar membrane, the spiral ligament, and the stria vascularis. Whereas most of this K^+ transport pathway is connected with gap junctions (10, 13, 35, 79), the steps between the hair cells and the epithelium, between the epithelium and the spiral ligament, and between the basal cells and the marginal cells in the stria vascularis are not. At each step, K^+ should be secreted from the former and absorbed by the latter. Finally, the marginal cells in the stria vascularis unidirectionally carry K^+ from the intrastrial space to the endolymphatic space, the scala media (37, 81, 83). Several K^+ transport apparatuses, including Na^+,K^+-ATPase, Na^+-K^+-$2Cl^-$ cotransporter (NKCC1), and K^+ channels (KCNQ1/KCNE1 and Kir4.1), have been identified expressed in the spiral ligament and/or stria vascularis. They are thought to play pivotal roles in cochlear K^+ circulation, because application of specific inhibitors for each apparatus reduced EP (24, 43, 47, 48) and targeted ablation of the genes for NKCC1 and the K^+ channels collapsed scala media (54, 81, 84). The K^+ channel Kir5.1, expressed in the fibrocytes in the lower part of the ligament, may negatively regulate K^+ circulation and may be important for precise control of K^+ flow (23).

It was recently reported that the gastric type H^+,K^+-ATPase is expressed in the cochlear lateral wall (49), but its details have not been studied. In this study, we have examined the precise cellular and subcellular localization of the H^+,K^+-ATPase in the cochlea and its functional role in EP formation. Using RT-PCR analysis, we found the expression of gastric α_1- and accessory β-subunits, but not of the colonic α_2-subunit, in

Address for reprint requests and other correspondence: Y. Kurachi, Div. of Molecular and Cellular Pharmacology, Graduate School of Medicine, Osaka Univ., 2-2 Yamada-oka, Suita, Osaka 565-0871, Japan (e-mail: ykurachi@pharma2.med.osaka-u.ac.jp).

[1] The online version of this article contains supplemental data.

The costs of publication of this article were defrayed in part by the payment of page charges. The article must therefore be hereby marked "*advertisement*" in accordance with 18 U.S.C. Section 1734 solely to indicate this fact.

cochlea. The α_1-subunit was specifically localized in particular types of fibrocytes in the lateral wall and the limbus, as well as at the basolateral site of marginal cells. Both perilymphatic and vascular perfusion of Sch-28080, a specific inhibitor of the gastric H^+,K^+-ATPase, suppressed EP. The unique distribution pattern and the pharmacological observations strongly suggest that the gastric-type H^+,K^+-ATPase plays a crucial role in cochlear K^+ circulation and thus in generation of the EP.

MATERIALS AND METHODS

Animals. The experimental protocol of this study was carefully reviewed and approved by the Animal Research Committee of Osaka University Medical School. All the experiments were carried out under the supervision of the committee and in accordance with Guidelines for Animal Experiments of Osaka University and the Japanese Animal Protection and Management Law. The animals were fed and allowed water freely until they were used for the experiments.

RT-PCR. Adult male C57 Black6 mice (~8–10 wk old) were deeply anesthetized with pentobarbital sodium (50 mg/kg). Total RNA was extracted from their whole cochlea, kidney, and distal colon with TRIzol reagent in accordance with the manufacturer's protocol (Invitrogen, Carlsbad, CA). DNase I was added to each 5 μg of RNA, and the mixture was incubated for 15 min at room temperature. After incubation, the mixture was treated with EDTA for 10 min at 65°C and then with proteinase K for 10 min at 65°C. RNA was purified with phenol and chloroform and then precipitated with ethanol. The RNA obtained was used to synthesize cDNA with oligo(dT) primers, one-twentieth of which was used for one PCR reaction. The DNA amplification was performed in a final volume of 30 μl. PCR cycling conditions were 94°C for 2 min, followed by 30 cycles of 94°C for 15 s, 57°C for 30 s, and 72°C for 45 s, with a final step of 72°C for 7 min. Amplified product (15 μl) was separated using electrophoresis in a 2% agarose gel and visualized with ethidium bromide. We analyzed transcripts of α_1-, α_2-, and β-subunits of mouse H^+,K^+-ATPase by primer pairs as following: the upstream primer 1F (5′-CTTCAGGAACAAGATCCTGGTGA-3′) and the downstream primer 1R (5′-GAAGGATAGATTCCCTCCAATGG-3′) for α_1, 2F (5′-CTTTGTTGCCATCATGGTCC-3′) and 2R (5′-GTATGCTTCACACAGTTTTC-3′) for α_2, and 3F (5′-CTTCAACAACCCCCATGACCC-3′) and 3R (5′-AGGACGGGCAAATGATCACAG-3′) for β.

Immunohistochemistry. All of the cochlear samples for immunohistochemistry were prepared as described previously (24). Viable dominant spotting (W^v/W^v) mice were purchased from SLC (Hamamatsu, Japan). Briefly, deeply anesthetized mice were perfused from their left ventricle with 4% paraformaldehyde-0.1 M sodium phosphate, pH 7.4, and cochleas were isolated. The cochleas were decalcified in EDTA solution (0.12% EDTA in PBS, pH 7.4) for 5 days.

An affinity-purified rabbit polyclonal antibody against gastric H^+,K^+-ATPase α_1-subunit was kindly provided by Dr. Noriaki Takeguchi (Toyama Medical and Pharmaceutical University) (2). The immunohistochemistry was performed as reported previously (26, 32). The cochlear cryosections (12 μm) were incubated with anti-α_1-subunit antibody (1:2,000 dilution) and fluorescein isothiocyanate (FITC)-labeled anti-rabbit antibody. Nuclei were detected using anti-heterochromatin 1γ (HP1γ) antibody (Chemicon, Temecula, CA) with Texas red (TXR)-labeled secondary antibody. The samples were examined under a confocal microscope (LSM 510; Carl Zeiss, Jena, Germany). We analyzed the expression of the α_1-subunit in cochlea of adult male rats and guinea pigs using the same procedure.

Isolation of cells from stria vascularis and cellular immunolabeling. The temporal bones of anesthetized mice were removed, and the stria vascularis was dissociated. Tissue strips of stria vascularis were incubated for 30 min at 25°C in a normal Tyrode solution (136.5 mM NaCl, 5.4 mM KCl, 1.8 mM $CaCl_2$, 0.53 mM $MgCl_2$, 5.5 mM glucose, and 5.0 mM HEPES-NaOH buffer, pH 7.4) containing 0.2% trypsin and then disrupted mechanically with pipetting (82).

Anti-barttin antibody, which was raised in chicken and affinity purified, was kindly provided by Drs. Shinichi Uchida and Sei Sasaki (Tokyo Medical and Dental University). Immunolabeling was performed using the same protocol as the slice immunohistochemistry described in *Immunohistochemistry*. The isolated cells were treated with anti-barttin (1:100 dilution), anti-α_1-subunit (1:2,000 dilution), and anti-Kir4.1 (1:2,000 dilution) antibodies and then visualized with FITC- or TXR-labeled secondary antibodies (see Fig. 3).

Immunoelectron microscopic examination. Preembedding immunoelectron microscopic analysis was performed as described previously (22, 26). Because the pigmentation in intermediate cells of C57 Black6 mice could be confused with immunoreactivity, we examined adult male ddY albino mice for this experiment. Anti-α_1-subunit antibody (1:100 dilution) was used to examine thin sections (thickness ~75–90 nm) of mouse cochlear lateral wall including the stria vascularis. The resulting immunoreactivity was visualized using the Vectastain Elite ABC kit (Vector Laboratories, Burlingame, CA) and 3,3′-diaminobenzidine.

Measurement of EP. Albino guinea pigs weighing 250–300 g were treated with pentobarbital sodium (50 mg/kg im) and vecuronium bromide (1.0 mg/kg im) and artificially ventilated with room air. The cochlea was exposed using a ventrolateral approach. We inserted a glass microelectrode filled with 150 mM KCl solution into the scala media of the second turn through the spiral ligament. EP was measured with an electrometer amplifier (FD223; WPI, Sarasota, FL). An Ag-AgCl wire placed in the thigh muscle served as reference. The recording system was zeroed with the electrode in the perilymph of spiral ligament before insertion into the scala media. Vascular perfusion of the stria vascularis was performed at a rate of 1.5 ml/min until the reaction became a plateau (~8–10 min) through a polyethylene tube located in the vertebral artery at the same side of the cochlea. Perilymphatic perfusion of the scala tympani was performed at a rate of 10 μl/min through a perfusion pipette connected to a syringe pump (UltraMicroPump II; WPI). The tip of the perfusion pipette was inserted into a small fenestration that was made in the bony wall of the scala tympani in the basal turn. The outlet for the perfusate was made at the top of the first turn. The artificial perilymph contained 126.0 mM NaCl, 5.0 mM KCl, 1.2 mM $CaCl_2$, 1.0 mM $MgCl_2$, 24 mM $NaHCO_3$, 0.5 mM NaH_2PO_4, 4.0 mM glucose, and 5 mM HEPES-NaOH buffer (34). Omeprazole (AstraZeneca, Osaka, Japan) was dissolved in control normal Tyrode solution or control artificial perilymph. The solution containing omeprazole, which is strongly alkaline, was adjusted to neutrality before its perfusion. Sch-28080 (Sigma, St. Louis, MO) was dissolved in methanol and stored at −20°C. Just before application, Sch-28080 was diluted in the control solutions, which also contained PUREBRIGHT MB-37 (10 mg/ml; Nippon Yushi, Tokyo, Japan). PUREBRIGHT MB-37 is a polymer-type solubilizer that is reported to be of low toxicity (44). The final concentration of methanol was <2%. The perfusion of either control Tyrode or artificial perilymph containing 2% methanol and 10 mg/ml PUREBRIGHT had no effect on EP (data not shown).

RESULTS

Expression of gastric type H^+,K^+-ATPase in mouse cochlea. The H^+,K^+-ATPase is classified into two types: gastric and colonic (nongastric). Two types of the α-subunit of H^+,K^+-ATPase, i.e., α_1 and α_2, have been identified. The functional H^+,K^+-ATPases are combinations of a catalytic α-subunit and an accessory β-subunit (14, 70). The assembly of the α_1- and β-subunits of the H^+,K^+-ATPase constitutes the gastric type proton pump (2, 63). On the other hand, the α_2-subunit of H^+,K^+-ATPase assembles with the β_1-subunit of Na^+,K^+-ATPase in native tissues such as epithelia of colon,

kidney, and prostate and forms nongastric type of proton pump, although the α_2-subunit can associate with the β-subunit of H^+,K^+-ATPase in vitro (8, 9, 45, 59, 60). To examine which subunits were expressed in cochlea, we performed RT-PCR analyses of total RNAs obtained from mouse whole cochlea, kidney, and colon with the primers specific for each subunit (Fig. 1).

Each set of the primers amplified a clear band when the total RNA of kidney or colon was used as a template (Fig. 1, *lane 1*). Using the same primers, we found that cochlea clearly expressed the mRNAs of α_1- and β-subunits (*lane 3*). On the other hand, the α_2 transcript was not detected in cochlear RNA (*lane 3*). The band of α_2 was not visible even when the PCR products were stained with SYBR Green I, which is ~25 times more sensitive than ethidium bromide to detect DNA (data not shown). All of the fragments depicted in Fig. 1 are specific, because PCR amplification of total RNA untreated with reverse transcriptase gave no signals (*lanes 2* and *4*). These results indicate that it is the gastric-type H^+,K^+-ATPase and not the colonic type H^+,K^+-ATPase that is predominantly expressed in mouse cochlea.

Distribution of H^+,K^+-ATPase in mouse cochlea. We next performed immunolabeling of cochlear cryosections with a specific antibody against the carboxy-terminal end of the α_1-subunit of gastric H^+,K^+-ATPase (2) and analyzed it on a confocal microscope (Fig. 2). The efficacy of this antibody was proven by specific and intense labeling of parietal cells in stomach (Supplemental Fig. 1),[1] as has been previously reported with other antibodies against α_1- or β-subunits of gastric H^+,K^+-ATPase (16, 20).

We first examined the labeling in mouse cochlea at low magnification. The antibody clearly labeled specific components of cochlear lateral wall (Fig. 2*A*, green). A moderate signal was detected in spiral ganglions as well (Fig. 2*A*). In the lateral wall, we observed strong α_1 immunolabeling in the lower part of spiral ligament, where type II and IV fibrocytes dominate, and also in stria vascularis, as reported previously (49). In addition, we detected clear labeling in the suprastrial zone and spiral limbus, where type V and another type of fibrocyte are respectively distributed (Fig. 2*A*). The regions with types I and III fibrocytes were free from labeling (Fig. 2*A*). A similar expression pattern for the α-subunit was also observed in cochleae of rats and guinea pigs (Supplemental Fig. 2). All of the reactions were specific, because no immunolabeling was detected when the antibody preincubated with excess immunized oligopeptide was used (data not shown). There was a faint signal in the tectrial membrane, which often shows nonspecific reactions (12, 64).

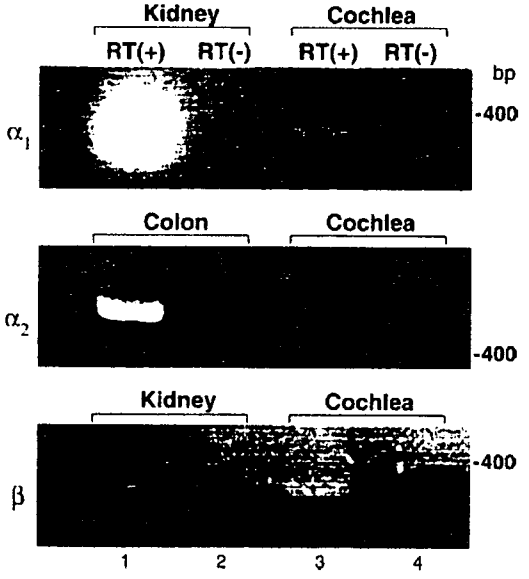

Fig. 1. RT-PCR analysis of H^+,K^+-ATPase subunits in mouse cochlea. Sets of primers specific for α_1-, α_2-, and β-subunits of H^+,K^+-ATPase were used for PCR reactions as indicated. Total RNAs obtained from kidney, colon, and cochlea were treated with (*lanes 1* and *3*) or without (*lanes 2* and *4*) RT and then amplified with the specific primers. PCR products were stained with ethidium bromide.

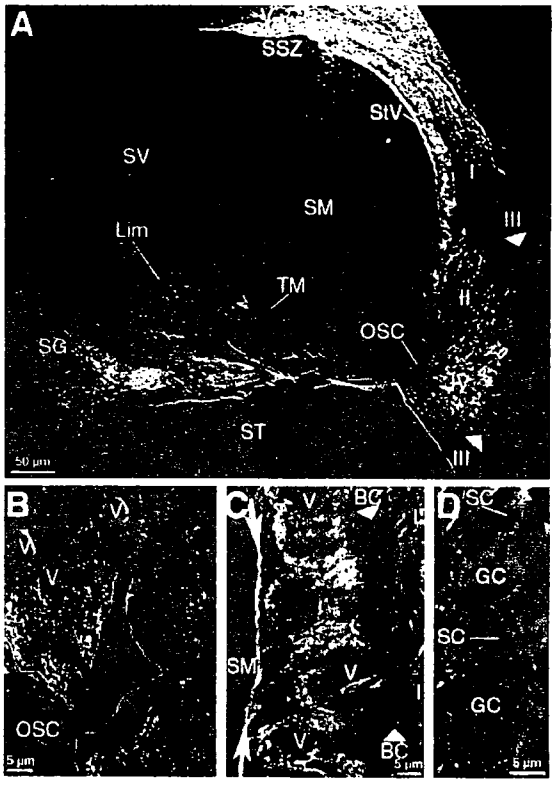

Fig. 2. Expression and distribution of H^+,K^+-ATPase α_1-subunit in mouse cochlea. Mouse cochlear sections were treated with an antibody specific to the α_1-subunit, and the immunoreactivity was visualized using FITC-conjugated secondary antibody. Images were obtained with a confocal microscope. *A*: low-magnification image. The α_1-subunit (green) was expressed in stria vascularis (StV), the lower portion of spiral ligament containing types II and IV fibrocytes, the suprastrial zone (SSZ) comprising type V fibrocytes, and spiral limbus (Lim). Moderate labeling also was detected in spiral ganglions (SG). Note that no signal was detectable in outer sulcus cells (OSC) or in the region of type I and III fibrocytes (arrowheads). SV, scala vestibuli; SM, scala media; ST, scala tympani; TM, tectrial membrane. Roman numerals indicate fibrocyte types. *B–D*: higher magnification images from different regions of the cochlea. In the lower part of the ligament (*B*), OSC and endothelial cells of blood vessels (V) were found to be free from α_1 labeling, indicating that the subunit was certainly expressed in the fibrocytes. The outline of the OSC is indicated by the white line (*B*). In stria vascularis, α_1 immunoreactivity was observed in the middle part, but at neither the apical side of marginal cells (*arrows*) nor in the basal cell (BC) layer (*C*, arrowheads). Moderate labeling also was visible in the cytosol of ganglion neurons (GC) but not in satellite cells (SC) (*D*). These sections also were stained with anti-heterochromatin 1γ antibody (red) to visualize the nuclei (*B–D*) (25).

We then examined the distribution of the α_1-subunit in spiral ligament and stria vascularis at a higher magnification. In the ligament, careful observation identified the "dot"-like labeling around ovoid or round nuclei that is associated with fibrocytes (Fig. 2*B*) (71). Labeling was not detected in either endothelial cells around blood vessels or outer sulcus cells (Fig. 2*B*). We therefore concluded that the α_1-subunit was expressed specifically in the fibrocytes of this region, i.e., types II and IV.

In stria vascularis, a strong signal was diffusely detected in its middle part, where basolateral membranes of marginal cells and apical membranes of intermediate cells are localized (Fig. 2*C*). No labeling was visible at either the apical site of marginal cells (arrows) or in the basal cell layer (arrowheads). As in the spiral ligament, we could not detect any α_1 immunoreactivity in endothelial cells in stria vascularis (Fig. 2*C*). These results strongly suggest that the α_1-subunit is localized at either the basolateral membrane of marginal cells or the apical site of intermediate cells. The resolution of confocal microscopic analysis was, however, insufficient to precisely determine the localization of the α_1-subunit, because the basolateral membrane of marginal cells and the apical membrane of intermediate cells are associated in close vicinity of ~150–200 Å and are prominently invaginated (28, 72). In spiral ganglions, we detected moderate labeling of the α_1-subunit in the neurons but not in satellite cells (Fig. 2*D*).

The RT-PCR study revealed that the cochlea expressed mRNA of the β-subunit of the H^+,K^+-ATPase (see Fig. 1). However, we could not detect any immunolabeling with commercially available anti-β-subunit antibodies. This may be due to either very low protein expression level of the β subunit in cochlea or loss of its antigenicity during the decalcification treatment (see MATERIALS AND METHODS).

Cellular and subcellular localization of H^+,K^+-ATPase in stria vascularis of mouse cochlea. We attempted to more precisely determine the localization of the α_1-subunit in stria vascularis at either the basolateral membrane of marginal cells or the apical membrane of intermediate cells. For this purpose, we first examined the viable dominant spotting (W^v/W^v) deaf mouse mutant, which is reported to lack intermediate cells in the stria vascularis (6, 76). As observed in the wild-type mouse (see Fig. 2), we still detected clear α_1 immunoreactivity in the stria vascularis of this mutant mouse (Supplemental Fig. 3, *A* and *B*), whereas the immunoreactivity of Kir4.1, which locates in intermediate cells, disappeared completely (Supplemental Fig. 3*C*). This observation suggests that the H^+,K^+-ATPase is expressed in marginal cells of W^v/W^v mouse.

We next prepared the cryosections of wild-type mouse cochlea again, and, in the stria vascularis, compared the localization of the α_1-subunit with that of either barttin, a constituent of a Cl^- channel selectively expressed at the basolateral membrane of marginal cells but not in intermediate cells (15), or Kir4.1, a marker protein for intermediate cells, using a double-immunolabeling technique. However, as expected, even at a high magnification under confocal microscopic analysis, the resolution of merged images was not enough to conclude which membrane expressed the H^+,K^+-ATPase (data not shown). This must be due to the fact that the basolateral membrane of marginal cells and the apical membrane of intermediate cells have abundant infoldings and are tightly associated together in very close vicinity, as mentioned above. Therefore, we isolated marginal and intermediate cells from stria vascularis of wild-type mice and examined the expression of the α_1-subunit of the H^+,K^+-ATPase in each cell type (Fig. 3).

Morphologically, marginal cells can be identified with their highly convoluted and infolded basolateral membrane (72). We also visualized barttin immunoreactivity as another hallmark for marginal cells (15). The barttin-immunopositive cells (Fig. 3*A*, green) possessed a highly convoluted and infolded basolateral membrane (arrowheads), ensuring that they were mar-

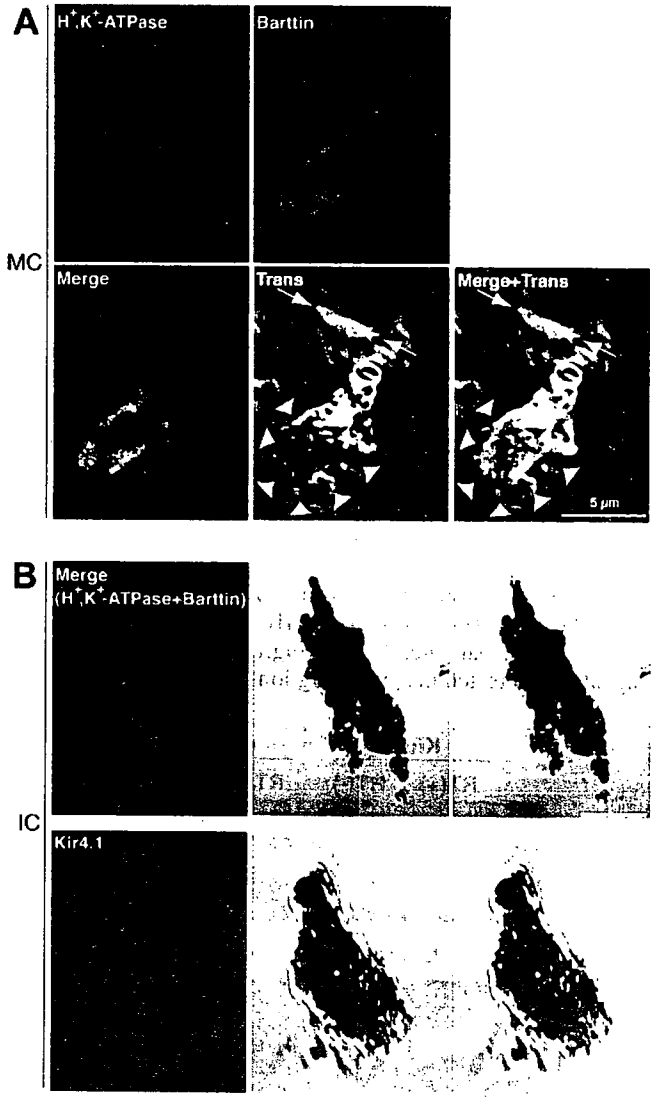

Fig. 3. Cellular distribution of the H^+,K^+-ATPase α_1-subunit. Cells were dissociated from stria vascularis of C57 Black6 mice, and immunolabeling was performed as described in MATERIALS AND METHODS. *A*: a marginal cell (MC). Double immunolabeling was performed with anti-α_1-subunit of H^+,K^+-ATPase and anti-barttin antibodies. The positive signals were visualized using Texas R (TXR; red)- and FITC (green)-conjugated secondary antibodies, respectively. A MC expressing barttin (green) (15) was α_1 immunopositive. The transmission illuminated images (Trans) show that the MC has a flat face on one side (arrows) and infoldings on the other side (arrowheads), which correspond to its apical and basolateral membranes, respectively (72). *B*: an intermediate cell (IC). Note that the cell is back-illuminated because of abundant pigments. Double labeling of α_1-subunit and barttin (*top*) and the single labeling of Kir4.1 (*bottom*) were performed with their specific antibodies. The intermediate cell was free from both α_1 and barttin immunoreactivity. Anti-Kir4.1 antibody (red) intensely labeled the cell, which ensures that it is an IC.

ginal cells. These cells were labeled with the anti-α_1-subunit antibody (Fig. 3*A*, red). Notably, labeling was detected at the basolateral side (arrowheads) but not at the apical membrane (arrows), of the marginal cells (Fig. 3*A*). Intermediate cells are a type of melanocytes (27, 82). Thus isolated intermediated cells could be identified with the melanin pigments. The cells with black pigments were devoid of either α_1 or barttin immunoreactivity (Fig. 3*B*, *top*), although they were clearly labeled with anti-Kir4.1 antibody (Fig. 3*B*, *bottom*, red) (1, 23). These results suggest that the H^+,K^+-ATPase is expressed in marginal but not in intermediate cells.

Finally, we conducted an immunoelectron microscopic examination on mouse stria vascularis (Fig. 4). Because it is often difficult in colored animals like C57 Black6 mice to distinguish the positive signal (black) of immunoreactivity from the pigmented inclusion bodies of intermediate cells, we examined the cochlea of albino ddY mice for this experiment. Marginal cells project their abundant basolateral processes to endothelial cells and pericytes of blood vessels (Fig. 4*A*). We detected prominent labeling of anti-α_1 antibody at the invaginated basolateral membrane of marginal cells (Fig. 4, *A* and *B*, asterisks). Little signal was visible on the apical site of these cells (Fig. 4*A*, arrows). Endothelial cells and pericytes were free from staining (Fig. 4*B*). We also carefully examined intermediate cells and their surroundings. The α_1-immunopositive infoldings of basolateral membrane of marginal cells (Fig. 4*C*, asterisks) tightly wrapped the soma and the processes of intermediate cells. The highly magnified images confirmed that the immunoreactivity was detected at the basolateral site of marginal cells (Fig. 4, *D* and *E*, asterisks) but not either on the somatic membrane (Fig. 4*D*, arrowheads) or at the projections (Fig. 4*E*, arrowheads) of intermediate cells. Accordingly, we conclude that the α_1-subunit of gastric H^+,K^+-ATPase is localized specifically at the basolateral membrane of marginal cells in stria vascularis.

Functional roles of gastric H^+,K^+-ATPase in cochlea. The distribution of gastric H^+,K^+-ATPase in the cochlea (see Fig. 2*A*) was found to be very similar to that of Na^+,K^+-ATPase and NKCC1 (11, 18, 36, 57, 67). This suggests that the H^+,K^+-ATPase may also be involved in cochlear K^+ circulation. To examine this possibility, we applied a specific inhibitor of gastric type H^+,K^+-ATPase, Sch-28080, to spiral ligament and also to stria vascularis. We used guinea pigs in this experiment, because this preparation is more suitable for electrophysiological measurement of EP. The expression of the α_1-subunit in guinea pig cochlea was confirmed with immunolabeling (Supplemental Fig. 2).

We first perfused the drug into perilymph to examine the role of the H^+,K^+-ATPase in the cochlear spiral ligament (Fig. 5). Sch-28080 decreased EP in a dose-dependent fashion (Fig. 5*D*). Sch-28080 (300 μM) dramatically decreased EP from +81.3 to +34.0 mV in 15 min in the example shown in Fig. 5*A*. Upon washout of the blocker, EP gradually returned to the initial level, indicating that its inhibitory effect is reversible (Fig. 5*A*). Sch-28080 (1 mM) suppressed EP more strongly, and the potential reached a negative value of −9.2 mV (Fig. 5*B*). These results suggest that the H^+,K^+-ATPase in spiral ligament is involved in formation of EP. On the other hand, perfusion of the perilymph with a high concentration of omeprazole (5 mM), an irreversible inhibitor of gastric H^+,K^+-ATPase that is active only in an acidic environment (<pH 5) (51, 89), had little effect on EP (Fig. 5*C*; n = 4). This may suggest that the extracellular fluid surrounding the strial H^+,K^+-ATPase is not acidic enough to activate the drug.

To examine the physiological function of the H^+,K^+-ATPase in stria vascularis, we applied Sch-28080 to a vertebral artery (Fig. 6), where the perfusate reaches the "intrastrial space" (see DISCUSSION), which is surrounded by the basolateral membrane of marginal cells and the apical membrane of intermediate cells (53). As reported previously (24, 53, 81), vascular perfusion of

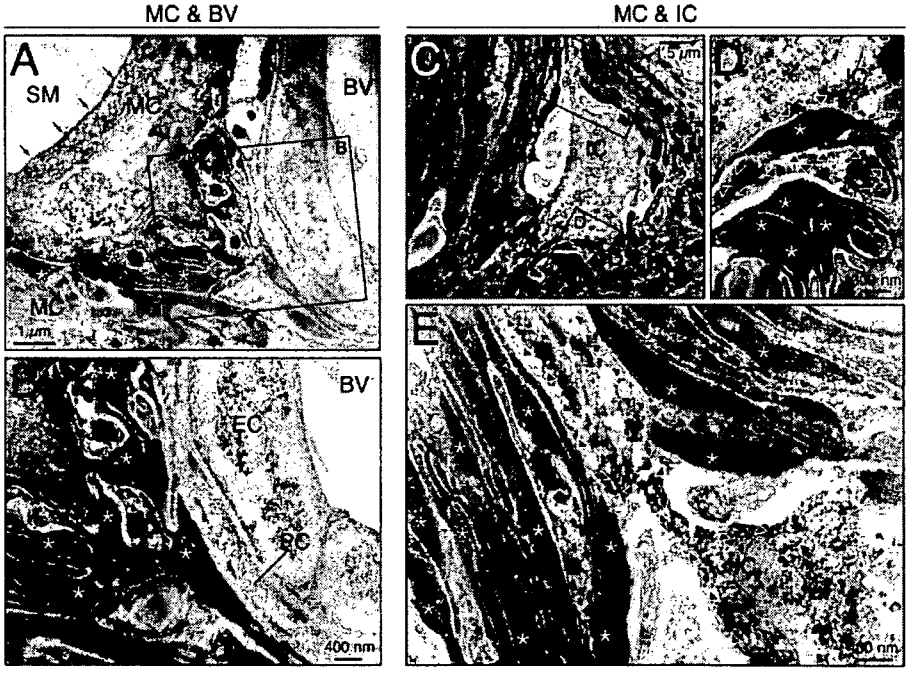

Fig. 4. Subcellular localization of the H^+,K^+-ATPase α_1-subunit in stria vascularis. This immunoelectron microscopic analysis was performed in stria vascularis of an albino ddY mouse with the antibody against the α_1-subunit. *A*: an area where a MC is closely associated with a blood vessel (BV). The *inset* in *A* is shown enlarged in *B*. Immunoreactivity was specifically detected at the invaginated basolateral membrane (*A* and *B*, asterisks) but not at the apical membrane (*A*, arrows) of the MC. Vascular endothelial cells (EC) and pericytes (PC) were free from staining (*B*). *C*: an area where the basolateral membranes of MCs twine around an IC. The *insets* in *C* are shown as higher magnification images in *D* and *E*. Arrowheads highlight the membrane of the IC. Whereas clear immunoreactivity was visible at the infoldings of basolateral membrane of MCs (asterisks), no positive signal was detected in the cell body or the processes of the IC.

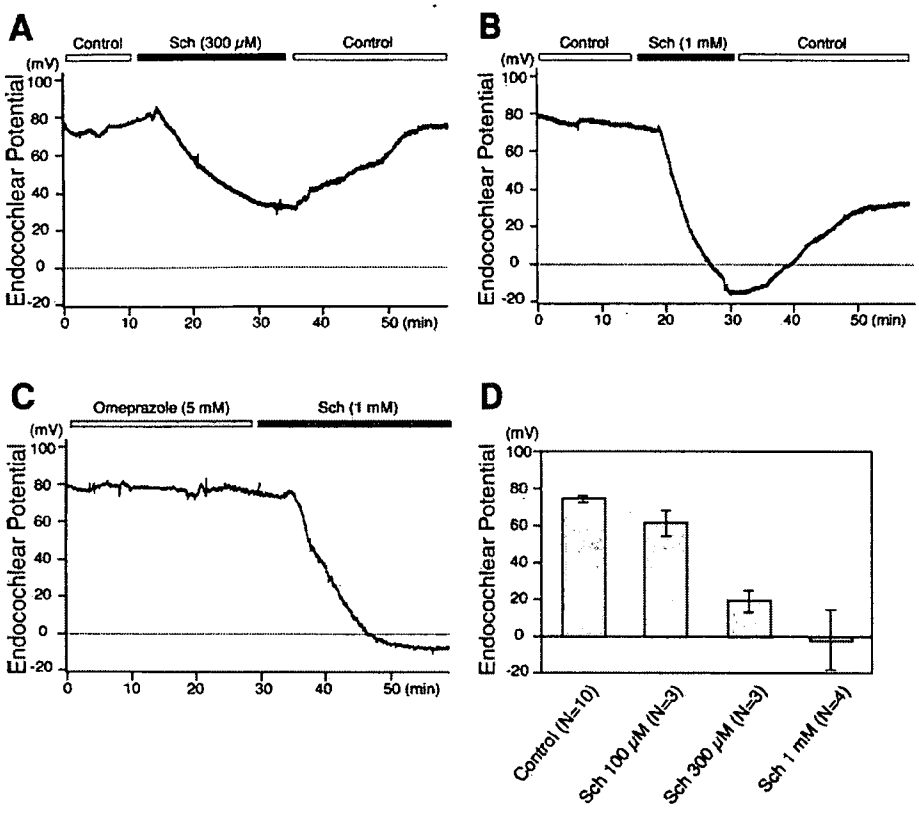

Fig. 5. Effects of perilymphatic perfusion of blockers of gastric H^+,K^+-ATPase on endocochlear potential (EP). The EP of guinea pigs was measured with perilymphatic (*A–C*) perfusion of blockers (Sch-28080 or omeprazole) specific for gastric H^+,K^+-ATPase. The blockers were applied for the periods indicated by horizontal bars, as described in MATERIALS AND METHODS. Sch, Sch-28080. *D*: dose-dependent reduction of EP by Sch-28080. Error bars represent SE.

Ba^{2+} (300 μM), a blocker of inwardly rectifying K^+ (Kir) channels, quickly suppressed EP (Fig. 6*A*). Sch-28080 (1 mM) strongly reduced the potential (Fig. 6*A*). A higher concentration (3 mM) of the drug completely suppressed EP (Fig. 6*A*). EP under administration into vertebral artery of Sch-28080 at 1 and 3 mM was +26.2 ± 7.4 mV (n = 5) and −7.7 ± 9.3 mV (n = 3), respectively (control: +75.8 ± 1.9 mV; n = 7) (Fig. 6*C*). Under the same conditions, the perfusion of up to 10 mM omeprazole had little effect on EP (Fig. 6*B*; n = 3). These results suggest that the gastric H^+,K^+-ATPase expressed in both spiral ligament and stria vascularis is functionally important in generation of the EP.

DISCUSSION

The major findings in this study are as follows. *1*) In the cochlear lateral wall, the gastric type but not the colonic type of H^+,K^+-ATPase was expressed in stria vascularis and in the fibrocytes of spiral ligament (49), spiral limbus, and suprastrial zone. *2*) In stria vascularis, the H^+,K^+-ATPase was expressed exclusively in marginal cells at their basolateral site, but not in intermediate cells. *3*) Inhibition of the H^+,K^+-ATPase in both stria vascularis and spiral ligament resulted in suppression of EP.

Specificity of Sch-28080 in inhibition of EP Sch-28080 is an inhibitor specific to gastric H^+,K^+-ATPase. In in vitro experiments using the vesicles isolated from stomach, gastric glands, and the human embryonic kidney (HEK) cells exogenously expressing α_1- and β-subunits of the gastric H^+,K^+-ATPase, it was reported that the IC_{50} value of the drug to inhibit the ATPase is ~0.2–5.2 μM and that ~100 μM of Sch-28080 is enough for complete inhibition (3, 85, 88). It was shown that at this concentration, the drug did not affect the activity of other transporters such as Na^+,K^+-ATPase and NKCC1 (4, 5, 7, 50, 68, 85, 92). In this study, we needed to perfuse 1 or 3 mM of Sch-28080 to the perilymph or the vertebral artery, respectively, to achieve complete suppression of EP (Figs. 5 and 6). It is therefore possible that the application of such high concentrations of Sch-28080 affected ion transport apparatuses other than H^+,K^+-ATPase and thus suppressed EP. Measurement of the actual concentration of Sch-28080 at the sites of action in cochlear lateral wall may be needed to reach the final conclusion whether the drug action is specific to inhibition of the H^+,K^+-ATPase. At present, however, it is technically very difficult to achieve this task, because the volume of the extracellular solution surrounded with invaginated basolateral membrane of marginal cells and that of the perilymph around infolded processes of the fibrocytes are very small (28, 71–73).

Nevertheless, on the basis of the relationship between the in vitro properties of other inhibitors and their effects on EP, we can roughly estimate the concentration of Sch-28080 in the lateral wall of living animals. For example, it was shown that total suppression of EP by inhibiting NKCC1 at the basolateral site of marginal cells or in the fibrocytes of the ligament required 1 mM of furosemide when applied through vertebral artery or perilymph (42, 47, 69), whereas 100 μM of furosemide was enough to completely inhibit the NKCC1 itself with the IC_{50} value of ~2.5–3.0 μM (66, 77). Thus the drugs in the perfusates are expected to be diluted to ~1/10 at the site of action in cochlea. Therefore, it would be the case that the actual concentration of Sch-28080 reaching the marginal cells in the stria or the fibrocytes in the ligament may be on the order